UNIVERSIDADE D
COIMBRA

Catarina Gonçalves Bispo

Design and fabrication of bioelectronic devices to measure electrical communication in neural networks

Dissertation in the context of the Master in Electrical and Computer Engineering, advised by Professor Henrique Gomes and presented to the Department of Electrical and Computer Engineering of the Faculty of Sciences and Technology of the University of Coimbra.

November 2024

FACULDADE DE CIÊNCIAS E TECNOLOGIA
UNIVERSIDADE D COIMBRA

Design and fabrication of bioelectronic devices to measure electrical communication in neural networks

Dissertation presented to obtain the degree of Master's in Electrical and Computer Engineering

Author
Catarina Gonçalves Bispo

Jury

President
Professor Gabriel Falcão Paiva Fernandes
Professor at the University of Coimbra

Supervisor
Professor Henrique Leonel Gomes
Professor at the University of Coimbra

Vowel
Professor Pedro Manuel Gens de Azevedo de Matos Faia
Professor at the University of Coimbra

Coimbra, November, 2024

Acknowledgements

Firstly, I would like to express my special thanks to my advisor, Professor Dr. Henrique Leonel Gomes, for his dedication and time throughout this journey and for generously sharing his vast knowledge. I must also acknowledge the contributions of all the other professors, researchers, and laboratory colleagues, along with the Instituto de Telecomunicações (IT).

I also would like to thank Dr. Rute Félix and Aliana Vairinhos from the University of Algarve, Inês Ponte from the University of Coimbra, and Gabrielle Coelho Lelis from the Brazilian Nanotechnology National LaboratoryLNNano, for all their help, availability, and friendship.

A special thanks to my lab colleague, Youssef Elamine, for all the help and advice on how to proceed with writing my dissertation and understanding the biological concepts.

I would also like to thank my family and friends, particularly my parents, grandparents, and godparents, for all their love, support, and patience during my academic journey.

This work was founded by FCT through the project AstroNeuroCircuit: Dispositivos Bioeletrónicos para medir a comunicação astrócito-neurónio **(Ref. n.º 2022. 06979.PTDC)**.

The work has been partially supported by the "Instituto de Telecomunicações (IT)". In the scope of the project, Catarina Bispo received a research grant with the **Ref.: B-0047-24**.

Abstract

The purpose of this dissertation is to develop a bioelectronic device with the ability to measure cell-to-cell communication, more specifically in the astrocyte population. The cell communication system under study involves one type of neuronal cell: astrocytes. Neurones are well-known brain cells that use electrical impulses, spikes, called action potentials (APs). However, astrocytes are the ones in control of the communication between neurons. Unlike neurones, astrocytes do not generate electrical spikes. Instead, they generate ultra-slow oscillations, or calcium signals, that can last for several seconds or even minutes. Because of their distinct bandwidths — APs measurements use a recording system in the kilohertz (kHz) bandwidth, and astrocyte signal measurements use a recording system in the millihertz (mHz) bandwidth — and the amount of studies about neurones, the lack of information about measurements of astrocyte signals presents a significant challenge in understanding how the brain works. Considering this gap, the project aims to develop a device that can accurately capture signals over various bandwidths with little noise.

The research included the fabrication of a bioelectronic device that includes five lanes of varying widths of gold and a circular electrode placed at the centre of Graphene Oxide (GO). The designed device and the commercial 8 Well PET Array (IBIDI device) with varying areas were used to capture extracellular signals using previously developed methodologies for extracellular electrical recording established by the research group hosting this thesis. These electrodes can detect small bioelectric oscillations in astrocyte populations. Despite their recording, the precise function of these oscillations remains unclear.

In order to better understand astrocyte communications, two hypotheses are proposed: (1) Astrocyte clusters synchronise to produce discrete extracellular electrical oscillations; (2) these synchronised oscillations propagate as electrical waves across connected cell populations. Two electrode types were employed: round electrodes (IBIDI device), to examine how electrode size affects extracellular signals, and fingered circular electrodes (fabricated device), specifically designed to detect travelling waves within the astrocyte network.Additionally, other experiments were conducted, and it was found that astrocytes generated signals in the nanowatt ($10^{-}9$ W) power range, with noise primarily being $1/f$ noise at low frequencies.

This thesis aims to enhance the field of bioelectronics by diminishing the knowledge gap between neurones and astrocytes. The findings not only enhanced the understanding of neural networks but also provided new, relevant information for the development of neuromorphic systems.

Keywords

Bioelectronics, astrocytes, neurons, action potentials, signal propagation, cell communication, extracellular communication, signal processing

Resumo

O objetivo desta dissertação é desenvolver um dispositivo bioelectrónico com a capacidade de medir a comunicação célula-a-célula, especificamente na população de astrócitos. O sistema de comunicação celular em estudo envolve um tipo de célula neuronal: os astrócitos. Os neurónios são células cerebrais bem conhecidas que utilizam impulsos elétricos, chamados APs. No entanto, são os astrócitos que controlam a comunicação entre os neurónios. Ao contrário dos neurónios, os astrócitos não geram impulsos elétricos. Eles geram oscilações ultra-lentas, sinalização de cálcio, que podem durar vários segundos ou mesmo minutos.Devido às suas larguras de banda distintas — as medições de APs utilizam um sistema de registo na largura de banda de kHz e as medições de sinais de astrócitos utilizam um sistema de registo na largura de banda de mHz — e à quantidade de estudos sobre neurónios, a falta de informação sobre medições de sinais de astrócitos representa um desafio significativo na compreensão do funcionamento do cérebro. Tendo em conta esta ausência de informação, o projeto pretende desenvolver um dispositivo que possa captar com precisão sinais em várias larguras de banda com pouco ruído.

A investigação incluiu o fabrico de um dispositivo bioelectrónico que inclui cinco pistas de diferentes larguras de ouro e um eléctrodo circular colocado no centro de GO. O dispositivo fabricado e o dispositivo comercial PET Array de 8 poços (dispositivo IBIDI) com áreas variáveis foram utilizados para captar sinais extracelulares utilizando metodologias previamente desenvolvidas para o registo elétrico extracelular implementado pelo grupo de investigação que acolhe esta tese. Estes eléctrodos podem detetar pequenas oscilações bioeléctricas em populações de astrócitos. Apesar do seu registo, a função precisa destas oscilações continua por esclarecer.

A fim de compreender melhor as comunicações astrocitárias, são propostas duas hipóteses: (1) os aglomerados de astrócitos sincronizam a sua atividade para produzir oscilações elétricas extracelulares distintas;(2) estas oscilações sincronizadas podem propagar-se por populações de células interligadas, formando uma onda elétrica. Foram utilizados dois tipos de eléctrodos: eléctrodos redondos, para examinar a forma como o tamanho do elétrodo afeta os sinais extracelulares, e eléctrodos circulares, especificamente projetados para detetar ondas de viajantes na rede de astrócitos.

Esta tese tem como objetivo melhorar o campo da bioelectrónica, diminuindo a diferença de conhecimento entre neurónios e astrócitos. Os resultados não só melhoraram a compreensão das redes neuronais, como também forneceram informações novas e relevantes para o desenvolvimento de sistemas neuromórficos.

Palavras-Chave

Bioelectrónica, astrócitos, neurónios, potenciais de ação, propagação de sinais, comunicação celular, comunicação extracelular, processamento de sinal

Contents

Acronyms

Ω	Ohms.
W	watts.
μm	micrometres.
μV	microvolts.
AC	alternating currrent.
APs	action potentials.
ATCC	America Type Culture Collection.
Ca^{2+}	Calcium ions.
Cl^{-}	chloride ions.
cm^2	cubic centimetre.
CNS	central nervous system.
CO_2	Carbon dioxide.
DEEC	Department of Electrical and Computer Engineering.
DMEM	Dulbecco's Modified Eagle's Medium.
DSA	Digital Signal Analyser.
ECG	Electrocardiogram.
ECoG	Electrocorticogram.
EDL	Electrical Double Layer.
EEG	Electroencephalogram.
EFs	endogenous electric fields.
EGG	Electrogastrogram.
EHG	Electrohysterography.
EMG	Electromyogram.
ENG	Electroneurogram.
EOG	Electrooculography.
EP	Evoked Potentials.
ERG	Electroretinography.
EVs	Extracellular Vesicles.
fECG	Fetal ECG.
FFT	Fast-Fourier Transform.
GABA	-aminobutyric acid.

GO	Graphene Oxide.
H^+	Hydrogen ions.
Hz	Hertz.
K^+	Potassium ions.
kHz	kilohertz.
LNA	low-noise amplifier.
MEAs	MicroElectrode Arrays.
mHz	millihertz.
mm	millimetres.
mV	millivolts.
Na^+	Sodium ion.
NaOH	Sodium hydroxide.
NYI	Not Yet Implemented.
OS	Operating System.
PCG	Phonocardiogram.
PET	polyethylene terephthalate.
PSD	Power Spectral Density.
s	seconds.
SiO_2	Silicon Dioxide.
SNR	Signal-to-Noise Ratio.
SR	stochastic resonance.
VCG	Vectorcardiogram.

List of Figures

List of Tables

Chapter 1

Introduction

The introduction aims at introducing the research line, the motivation, and the outcomes of this dissertation. This project aims to develop a bioelectronic device capable of measuring cell-to-cell communication, focusing on the detection and analysis of extracellular bioelectrical signals. This chapter delineates the structure of the dissertation, offering a summary of the content in each following chapter.

1.1 Motivation and objectives

The field of neuroscience has been extensively studied due to its fundamental role in a comprehensive understanding of brain functionality in health and disorder, making it possible to develop targeted treatment strategies. The research line is also attracting the attention of electrical engineers and computer scientists, who approach it as a fundamental layer in developing innovative machine learning and computational strategies [1, 2, 3].

Neurons, at the core of central nervous systems, are the well-known messenger cells of the brain that communicate through spikes known as action potentials (APs) [4]. However, neural communication is not only the responsibility of the neurons. Astrocytes are a type of glial cell that plays a fundamental but less known role in neural networks. Unlike neurons, astrocytes use a more subtle language of ultra-slow oscillations, creating a series of signals that can last several seconds or minutes[5, 6].

The study of these two cell types presents an engineering problem. The strong contrast in their modes of communication-electrical spikes in neurons and very slow oscillations in astrocytes-requires a measurement approach that can be used for both. The measuring techniques that exist can capture the fast APs of neurons in the kilohertz (kHz) bandwidth. However, they are unable to record the astrocyte signals, which reside in the millihertz (mHz) bandwidth [7]. This discrepancy in signal bandwidths highlights a significant gap in our ability to fully understand and measure the dialogues within the brain's cellular network. This occurs due to the general focus of the electrophysiological scientific community on the quantification of neural communication.

In a way of fixing this lack of information about astrocytes and the lack of electrical techniques to measure these types of cells *in vitro* (engl: in the glass), electronic devices have been developed. These devices have evolved with the micro- and nanotechnologies. These technologies have allowed the creation of smaller components like sensors. Despite this progress, there is still a lack of a reliable device capable of measuring multiple signalling domains. Hence, the focus of this dissertation is to develop the design of a bioelectronic device that effectively connects several signalling domains with high accuracy. The proposed device will help with the integration of both neuronal and astrocytic cells within a network, while also including a recording system with two different bandwidths. This device will be optimised to accurately detect the spikes of neurones and the prolonged oscillations of astrocytes, while also maintaining a very low level of interference to ensure the high quality of the recorded signals. By providing more information about how astrocytes communicate with each other, this thesis aims to enhance neurologists' understanding of neuronal communications and increase their understanding of the functionalities of these cells, enabling their implementation in neuromorphic circuits.

1.2 Outcomes for the design of neuromorphic circuits

The findings of this project could have implications for progress of neuromorphic systems. These systems are analogue circuits that mimic the intelligence, learning, and memory capabilities of the brain.

Neuromorphic circuits have successfully incorporated astrocyte-like functions to simulate and emulate their role in the phase synchronization of neuronal activity. By mimicking the behaviour of astrocytes, these circuits have the ability to control synaptic activity and facilitate synchronous neuron firing spikes. This enhances the performance and efficiency of neuromorphic circuits. Neuromorphic systems of this kind have the capacity to influence the synchronisation of neuronal phases, which is crucial for maintaining coherent neuronal activity patterns and enhancing the computational capabilities of these systems. [1].

Self-repair strategies for electronic circuits have been influenced by astrocytes. Astrocytes are responsible for the repair of faulty synaptic connections between neurons, and this capability has been mimicked in this circuits. By incorporating of astrocyte-driven repair process into hardware, neuromorphic circuits can address the problem of faulty synapse, which will enhance their reliability and lifetime. This is extremely important for reducing problems related to geometric scaling, wear-out and manufacturing defects [2].

On the other hand, neuromorphic systems may also provide feedback to neuroscientists by reverse engineering the brain. Since the interaction between neurons and astrocytes in these circuits can offer valuable feedback to neuroscientists, which helps them understand the functionalities of the brain and diseases in more detail. This way, both fields of researchneuromorphic systems and neuroscientists, gain a better practical framework for studying complex neural processes.

The digital implementation of neuron-astrocyte interaction for neuromorphic applications goes beyond theoretical models. Models that simulate the brain's functions are already being implemented. In the paper [3], a new model was presented that demonstrates the interaction between spiking neuron networks and astrocytes to improve working memory capabilities. Using this model, it was observed that astrocytes can store traces of neuronal activations for several seconds, modulating synaptic connections during the retrieval stage, and consequently enhancing memory recall.

Neuromorphic engineering is particularly useful for hardware that interacts with the physical world, such as biological systems, sensory data, or prosthetic devices, where small size and low power consumption are extremely important.

1.3 Dissertation organisation

The thesis is structured into eight chapters, with each chapter dedicated to a specific topic of the project. Following the introductory chapter, which presents a comprehensive summary of the thesis and it is motivation, the subsequent chapters are structured in the following manner:

Chapter 2 delineates the current advancements in the field, along with a brief summary of the scientific community's efforts to improve their understanding of brain performance. This chapter examines the current technology and methods used in measuring electrical communications in neural networks. It also evaluates the limitations of existing bioelectronic devices and emphasises the need to enhance understanding of astrocytes within brain networks.

Chapter 3 describes the equivalent circuit that models the interface between cells and the sensing electrode. This chapter also lays out the concepts relevant to this study by introducing the biological basics of extracellular signals and the noise in bioelectrical activity measurements.

Chapter 4 focuses entirely on the materials and methods used in conducting the studies on cell cultures. This chapter provides a description of sensing structures that establish a physical link between two interfaces, thereby transforming the signal from one interface into an equivalent signal with the mobility characteristics of the second interface. The chapter will also explain the technologies used to capture extracellular communications. Additionally, this chapter provides a description of the biological material used in this study.

Chapter 5 focuses on the classification and analysis of the different bioelectrical signals recorded during experiments with astrocytes. The chapter further presents a signal that is equivalent to the typical one seen in this study. Using this equivalent signal for calculating its power facilitates determining the order of magnitude of the usual bioelectrical signals in this research.

Chapter 6 is focused on the analysis of the effect of electrode geometry and material on the signal captured. This analysis explores the bioelectrical activity generated by a population of astrocytes, which allows for the study of whether the observed electrical oscillations are travelling waves or localised activities. Ini-

tially, it also gives a brief description of the sensing electrodes and the methods used in this study.

Chapter 7 explores the analysis of electrical noise within astrocyte populations. This chapter used long-term recordings to explore bursts of bioelectrical activity interspersed with periods of silence, both in the time and frequency domains. The investigation of trigger signals, also known as master signals, provides insights into the cell's signal coordination. Additionally, it provides a brief description of the GO electrode.

Finally, Chapter 8 summarises the research's conclusions, emphasising the key discoveries and knowledge gained. The chapter also addresses the problems that surfaced during the study and suggests potential solutions to resolve some of them.

Chapter 2

State of the art

This chapter reviews the current methodologies and devices used to measure electrical communication in biological cells. It offers an overview of the scientific disciplines contributing to the study of electrical communication in biological cells, focusing on techniques for recording extracellular bioelectrical signals. The discussion emphasises the advantages and limitations of these approaches and underscores the need for developing novel technologies to address cell-cell communication, particularly in non-nervous cells.

2.1 Introduction

The concept of bioelectricity is primarily associated with specific types of cells, most notably cardiac cells, which generate the cardiac impulse, and nerve cells, which transmit signals from and to the central nervous system (CNS). In this last case, complex neural networks, composed of various neurons, coordinate and process information in the CNS. Neurons are in the core interest of research focusing on electrophysiology of the CNS due to their ability to generate electrical impulses, known as action potentials (APs). The interest of the neuroscience community on understanding how APs are generated and transmitted across intricate neural networks involving hundreds of neurons, comes from three reasons: First, APs are signals that allow neurons to communicate with each other across synapses, enabling all neural processes from sensory perception to complex cognitive functions. second, many neurological and psychiatric disorders, like epilepsy, schizophrenia, and Parkinson's disease, are linked to abnormalities in action potential generation and propagation. Third, and importantly, measuring APs is relatively straightforward compared to other neural signals. This ease comes from their distinct electrical nature, which allows scientists to use microelectrodes to directly record the rapid voltage changes during APs. In fact, bioelectricity is not restricted to cardiac and neuronal cells. Back in the 18^{th} century, bioelectricity was also linked to other types of cells, namely skin cells in dermal wounds, with early researchers discovering that skin injuries produced small electrical fields. Despite this early insight, the role of bioelectricity in other tissues outside the nervous system and the brain has largely been overlooked.

The importance of neuronal APs and the ease of their measurements have distracted the attention of the scientific community from other types of cells in the CNS. For instance, Glia cells, astrocytes in particular, were regarded as supportive cells to neurons since they have proven roles of maintaining ion and neurotransmitter balance in the extracellular space and ensuring neurons have the energy needed for proper functioning. Although it is accepted that astrocytes do not general APs, new studies reported that astrocytes are also electrically active, and highlighted their importance in the well-functioning of the CNS. To highlight the magnitude of the role astrocytes play in the CNS, it is worth noting that a protoplasmic astrocyte can contact between 270,000 and two million synapses, in humans. In addition, astrocytes are highly interconnected via gap junction, allowing an internal flow of information. therefore, studying the synergies between astrocytes and neurons has become the focus of many communities. [8, 9, 10].

In recent years, two distinct scientific communities have shown increasing interest in astrocytes: (a) neuroscientists and (b) the neuromorphic engineering community. Neuroscientists are focused on unravelling the role astrocytes play in neural communication, while the neuromorphic community seeks inspiration from the brain to develop electronic circuits and computational algorithms that move beyond binary systems.

The neuromorphic community quickly recognised the value of incorporating a second cell type to regulate signal flow across synapses. As a result, astrocytes have recently been integrated into artificial circuit designs to enhance the functionality of neuromorphic circuits [1, 2, 3]. This concept is briefly explored in the section 1.2 . In parallel, several research groups, including the team hosting this thesis, have become increasingly interested in the bioelectrical activity of astrocytes, particularly in how these cells interact electrically with neurons. To advance this understanding, these groups are developing and fabricating novel devices that guide neurons and astrocytes to form precise, interconnected networks on a chip. These devices enable the detailed observation of spatial movement and signal exchange between cells, providing deeper insights into their interactions. After providing a brief overview of the scientific communities interested in neural networks formed between neurons and astrocytes, this chapter provides to the reader the background information about the various extracellular recording techniques. Furthermore, it provides a succinct explanation of the bioelectronic devices currently in use.

2.2 Recording techniques

The electrophysiological scientific community has primarily concentrated on recording neural communications, leading to the development and improvement of several techniques.

Two primary types of technologies are used to record cell signals: (a) the patch clamp method and (b) extracellular electrodes.

The patch clamp method probes exclusively punctual ion channels or, at most, one individual cell, examining specific ion channels across the cell membrane.

While it provides critical insights into the functioning of these channels, the method is invasive, does not offer information about cell-to-cell communication, and cannot be applied to networks of cells.

To study intercellular communication, extracellular electrodes are used instead. These electrodes measure the collective extracellular electrical activity resulting from ionic movements across cell membranes, allowing researchers to probe ensembles of cells and their interactions within a network. The sections below describe the two technologies and their advantages and limitations.

(a) Patch-Clamp Techniques

Patch-Clamp technique permits researchers to measure ionic currents flowing through individual ion channels in cell membranes or across the membranes of excitable cells[11, 12, 13]. This technique, developed in the late 1970s and early 1980s, uses a glass pipette with an extremely narrow tip. This pipette is carefully attached to a small section of the cell membrane, forming a high-resistance seal called a "gigaseal". The term "seal resistance" is commonly used to refer to the electrical resistance between the cell and the surrounding solution (also known as ground) [7]. The "gigaseal" facilitates the manipulation of membrane potential and ionic environment on both sides of the membrane, making it simple to generate electrical signals at the single-channel level.

Figure 2.1 shows the following configurations are possible with the patch-clamp technique:

- Cell-attached configuration is used to study ion channels while preserving the intracellular environment;

- Inside-out and outside-out patch configurations allow the manipulation of the ionic environment;

- Whole-cell configuration enables the measurement of currents across the entire cell membrane.

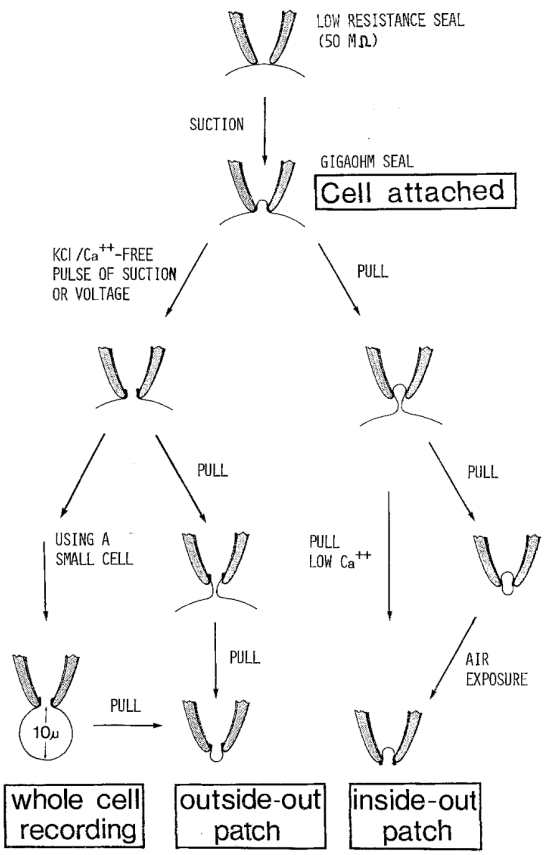

Figure 2.1: Schematic representation of the procedures that lead to recording configurations[14].

All these configurations have contributed to understanding cellular excitability, synaptic transmission, and pharmacological characteristics of ion channels. As such, patch-clamp has become an unavoidable tool for the investigation of excitable cells, such as neurons, muscle fibers, and cardiomyocytes.

Two acquisition modes are available for parch clamping: the current clamp and the voltage clamp. The current clamp technique rely on regulating the current passing through the membrane and records the resulting changes in membrane voltage, typically observed as APs. In contrast, the voltage clamp technique is a measurement of currents resulting from the establishment of a predetermined level of membrane voltage.[15]

Although astrocytes were not regarded as electrogenic cells, researchers conducted studies on the use of patch clampt to investigate channels of this cell type. For instance, in 1986, F.N Quandt and B.A. MacVicar analysed single channel currents in intact and excised patches of glial cell membranes developed in primary cultures taken from newborn rate brains. The researchers confirm that Calcium ions (Ca^{2+})-activated Potassium ions (K^{+}) channel is present in the membrane of astrocytes grown in culture. This finding, along with the evidence indicating that the Ca^{2+} channel is dependent on voltage, supports the notion that glial cells play a crucial role in controlling excitability in the CNS. Furthermore, the study

shows that when depolarisation occurs, the influx of Ca^{2+} would enhance the permeability of the membrane to K^+ and could increase the "buffering" capacity of the glial cells for extracellular K^+.[16]. Other researchers reported that the -aminobutyric acid (GABA) receptor channels in astrocytes have similar characteristics to those observed in neuronal cell membranes. Some of the results obtained using patch clamp indicated a non-uniform distribution and possible clustering of GABA receptors on astrocyte surfaces, which may influence the "buffering" of chloride ions (Cl^-) activity in the extracellular environment.[17]

In a more recent study [18], the researchers used the patch-clamp technique's whole-cell configuration to investigate the impact of astrocyte activity on the effects of ketamine, a general anesthetic, on spontaneous postsynaptic currents (SPSCs) in S1 pyramidal neurones. It was concluded that astrocytes have an impact on the effects of ketamine on both pre- and postsynaptic components, therefore contributing to synaptic transmission.

(b) extracellular electrodes

The study published in [6] comes to the conclusion that, while the patch-clamp technique is appropriate for measuring individual cells, it is not ideal for measuring astrocyte populations. However, the patch-clamp technique made possible to understand that each living cell acts like a signal generator.

The sharp electrode technique is used to perform intracellular recording from neurons. In the next section, the sharp electrode will be briefly mention.

The recording technique using MicroElectrode Arrays (MEAs) includes the use of an array of small electrodes to detect and record the electrical activity of neural networks *in vitro* (engl: in the glass) [19]. The following section will provide a more detailed explanation of the electrodes used in this technique.

2.3 Bioelectronic Devices

Over the past few years, there has been rapid growth in the development of electronic devices designed for medical and biological applications. These devices have made significant contributions to the advancement of healthcare and the expansion of knowledge about the human body, specifically the brain. These tools are valuable for monitoring and measuring both *in vitro* (engl: in the glass) and in vivo physiological responses. This progress has been further accelerated by advancements in nanofabrication, which involves the super miniaturisation of electronic circuits and mechanical structures. Advancements in technology have made it possible to create smaller, more targeted, and more efficient bioelectronic devices that can connect with living tissues, cells and organs. [20]

The electrodes are essential components in the bioelectronic devices discussed in this dissertation, as they have an important function in measuring cell activity. Previously discussed recording techniques, such as patch-clamp, generally require the insertion of electrodes into different biological tissue preparations.

These techniques use the following main types of electrodes:

1. Basic solid conductors, such as discs and needles (either individual or grouped together, usually with insulation covering except for the pointed end);
2. Tracings on printed circuit boards are insulated, except the tip;
3. Hollow tubes filled with an electrolyte, such as glass pipettes containing potassium chloride or another electrolyte solution.

[15]

Sharp electrodes are tools with high impedance that are used for intracellular recording, particularly in small neurons, as previously mentioned. Although they are effective, they present challenges such as limited membrane penetration, resulting in a burst of spikes and sustained depolarisation of the neuron. The presence of these electrodes can also result in a decrease in input resistance and reduce spike amplitudes as a result of their low-pass filtering effect.[21]

MEAs are devices composed of a grid of electrodes, usually fabricated on a substrate, designed to interface with cultured cells or brain slices. The use of this devices showed more progress because they were better at keeping an eye on individual cells and making it easier for electrogenic cells to talk to each other [22, 23, 24, 25]. Using electrodes with a small surface area allows for spatial resolution, enabling the identification of the specific neuron responsible for generating an action potential.

Furthermore, few research groups have also focused on studying astrocytes using extracellular microelectrodes. Several research groups have employed MEAs for this particular purpose. For instance, the authors of [26] documented the application of planar MEAs to measure the spontaneous electrical activity of isolated astrocytes. For the first time, they discover slow oscillatory activity. Furthermore, they also observe the differences in the impact of drugs on primary astrocytes and iPSC-derived astrocytes. This shows that MEAs could be used to study how drugs affect astrocytes.

In the same way, the researchers in [27] employ a PDL pre-coated 24-well MEAs plate (Axion Biosystems) equipped with 16 microelectrodes arranged in a grid of 4×4 in each well to record extracellular electrical activity. An objective of this work is to characterise the Extracellular Vesicles (EVs) cargo proteins derived from primary astrocytes (ADEVs) under both physiological (normal) and pathophysiological (diseased) states. Through their discovery, a deeper understanding of the functions of astrocyte EVs was achieved. This knowledge is believed to contribute to the advancement of new diagnostic and therapeutic possibilities for neuroinflammatory disorders such as Alzheimer's disease and Parkinson's disease.

On the other hand, other groups employ different types of microelectrodes. For example, in [28], the authors show a microelectrode that was specifically created to measure the flow of Hydrogen ions (H^+) in the extracellular environment from individual astrocytes. This study investigates the influence of extracellular

ATP on an increase in H^+ flux from astrocytes. The findings suggest that ATP-mediated extrusion of H^+ from astrocytes can have a significant impact on the regulation of electrical signals in the nervous system.

The Utah Array is a small device consisting of multiple electrodes that are used to record neural activity inside the body, specifically in brain-computer interface applications. The device contains 100 microneedles, allowing precise and detailed recordings of neural activity. The Utah Array is highly advantageous for its accurate neural targeting. Still, it is also vulnerable to limitations such as tissue encapsulation and degradation of recording quality over time due to the biological response[29, 30, 31].

It is important to mention that when operating in voltage detection mode, the thermal noise originating from an electrode becomes increasingly noticeable as the electrode dimensions decrease [**?**]. As previously stated, non-electrogenic cells such as astrocytes cannot generate action potentials, unlike electrogenic cells[32]. However, they still have mechanisms to transport ions across their cell membranes[33].

2.4 Conclusions

In summary, two electrophysiological techniques are used to measure electrical impulses generated by cells: the patch clamp method and extracellular electrodes.As previously stated, the patch clamp technique provides detailed insights at the single-cell level, but it is too invasive to the cells and limited in terms of capturing extracellular communication.

Recent advances in materials and microelectronic fabrication have enabled the development of miniature arrays consisting of thousands of electrodes, commonly referred to as MEAs. MEAs have revolutionised the study of neural networks by allowing researchers to decode the complex ensembles of APs exchanged between neurons during communication.

However, commercially available MEAs are specifically optimised for neurons and, as a result, are unable to detect signals from cells that do not generate action potentials. A good example is the astrocyte cell, which does not produce APs.

Even though these limitations exist, the scientist became more interested in astrocytes and what role they play in the brain. This led to an improvement of MEAs and other extracellular microelectrodes adapted to record astrocyte cell signals.

The earlier studies talked about in this chapter show that MEAs are getting better because they were used to slow oscillatory activity, characterise EVs cargo, and detect H^+. These researcher's findings contributed to an understanding of astrocyte functions.

Considering the significant focus on astrocyte cells, it is important to develop bioelectronic devices that can accurately measure the electrical activity of astrocytes. Further development of recording techniques is necessary to enhance the accuracy of capturing astrocyte activities using these devices. This technological progress would not only enable the growth of neural network understanding but

also enhance the identification and treatment of neurological disorders.

In this chapter, we review the current technologies used to measure astrocytes, highlighting some studies that have successfully captured extracellular communication.

Chapter 3

Fundamentals

This chapter aims to provide an overview of the fundamental concepts and terminology used throughout this thesis. Initially, it will be provided a brief explanation of the biological aspects related to the origin of extracellular signals, with a particular focus on astrocytes. Following this, an equivalent circuit that describes the interface between cells and the sensing electrode is presented, focusing on the Electrical Double Layer (EDL). The chapter ends with an explanation of the importance of noise in bioelectrical activity, describing noise evaluation and two types of noise: thermal noise and $1/f$ noise.

3.1 Introduction

This chapter aims to explain the key concepts, which will be mentioned throughout this document. Since this dissertation focuses on the study of the interface between living cells and electronic devices, the following section will provide discussions of how it is possible to capture signals generated by cells with electronics and how electronics can interfere with this recording.

The main electronics in this work are the bioelectronic devices. They can monitor and regulate the interior environment of biological objects in real-time, making them ideal for therapeutic and implantable biomedical applications, including drug delivery, electrophysiological recording, and regulation of intracellular activities [34, 35].

An equivalent circuit is presented to facilitate the description of the electrical coupling between the cell and the sensing electrode. The EDL, also known as the Debye-Helmholtz layer, is formed at the interface between a conductive material and a conductive solution. Ions in the conductive solution facilitate the movement of electrical charges between the electrode and the cells. This solution is also known as an electrolyte medium. This solution serves as the environment for the transmission and capture of cell signals. This layer is an extremely thin layer, normally just a few nanometres thick, that acts as a dipole layer, which consists of ions on the electrolyte side and electrons (e^-) on the electrode side.

This thesis mainly investigates glial cells, known as astrocytes. The investiga-

tion of these cells aims to reduce the deficiency of knowledge about them, trying to explain their signal generation, their function within neural networks, and the differentiation from neurones, the other kind of neural cell. This thesis will investigate extracellular signals, specifically the alternating currrent (AC) signal type, to gain this knowledge.

3.2 Biological background

The biological field studies all living species, all of which originate from a unicellular ancestor that originated about 4 billion years ago [36]. In this thesis, the term "cells" is the most relevant biological term. Hooke first used the term during his study of cork microstructures in 1665, using optical equipment with a 30X magnification capability [37].

Further discoveries and technical advancements have enabled the microscopic study of cells and the growth of knowledge about them. This thesis attempts to clarify the role of astrocytes — a kind of glial cell within the neuronal network of the brain — with an emphasis on their extracellular signalling activities.

3.2.1 Electrogenic cells and non-electrogenic cells

The primary objective of this thesis is the eukaryotic cell known as the astrocyte. Eukaryotic cells possess a nucleus and membrane-bound organelles. It is mostly multicellular and has a considerable size, ranging from 10 to 100 micrometres (μm). This living thing is complicated, and its DNA is linear [38].

Biologists classified these cells into two categories: electrogenic and non-electrogenic cells. Electrogenic cells generate electrical impulses, such as action potentials (APs) or cardiac impulses. Some of these cells are neurones, nerve cells, and cardiac cells. On the other hand, non-electrogenic cells, such as astrocytes, lung cells, and skin cells, do not generate individual electrical spikes [39]. Even though these cells are classified as non-electrogenic, most of them in their membrane have a complex machinery of pumps, transporters, and ion channels that enable the exchange of ions with the extracellular environment, which allows them to produce voltage fluctuations in the environment surrounding them.These charges produce electric fields named endogenous electric fields (EFs), which often coordinate ionic exchanges to create electrical oscillations or waves capable of spreading across biological tissue. These electrical oscillations are very slow and may last for many seconds or even minutes. In contrast to APs that spread at a velocity of meters per second, a calcium wave (ultra-slow oscillations) propagates at a speed of μm per seconds (s).

To better understand the difference between electrogenic cells and non-electrogenic cells, it will briefly explain one cell of each type: (a) neurones, which are electrogenic cells, and (b) astrocytes, which are non-electrogenic cells.

(a) Neurones

The nervous system has 80 to 100 billion neurones essential for the transmission of information via electrochemical signals. The structure of a neurone comprises a cell body, dendrites, and an axon. The axon transmits signals to other neurones or effector cells, while the dendrites receive signals from other neurones [40].

Neurones have the ability to form complex communication networks that enable all brain functions, such as elaborate processes like memory and more simple functions like breathing.

As mentioned before, these cells are considered electrogenic cells because they generate APs, which only have a duration of milliseconds and are commonly known as spikes.

The electrophysiological scientific community has focused on neurones for many years, paying particular attention to the recording of APs.

(b) Astrocytes

Astrocytes are named after their structure, with 'astro' meaning star and 'cytes' denoting cells. These cells have a star-like shape with many branches that facilitate connecting synapses between neurones. Synapses are junctions between two neurones, where neurotransmitters facilitate communication. Upon the arrival of an action potential at the presynaptic neurone's terminal, calcium channels open, initiating the release of neurotransmitters into the synaptic cleft [41]. These neurotransmitters connect to receptors on the postsynaptic neurone, triggering a reaction. Afterwards, neurotransmitters are either recycled or destroyed to prevent overstimulation, thus ensuring accurate signal transmission and maintaining the equilibrium of neuronal activity [42]. An individual astrocyte can interact with thousands of synapses, enabling it to simultaneously affect several neurones (see Figure 3.1(c)).

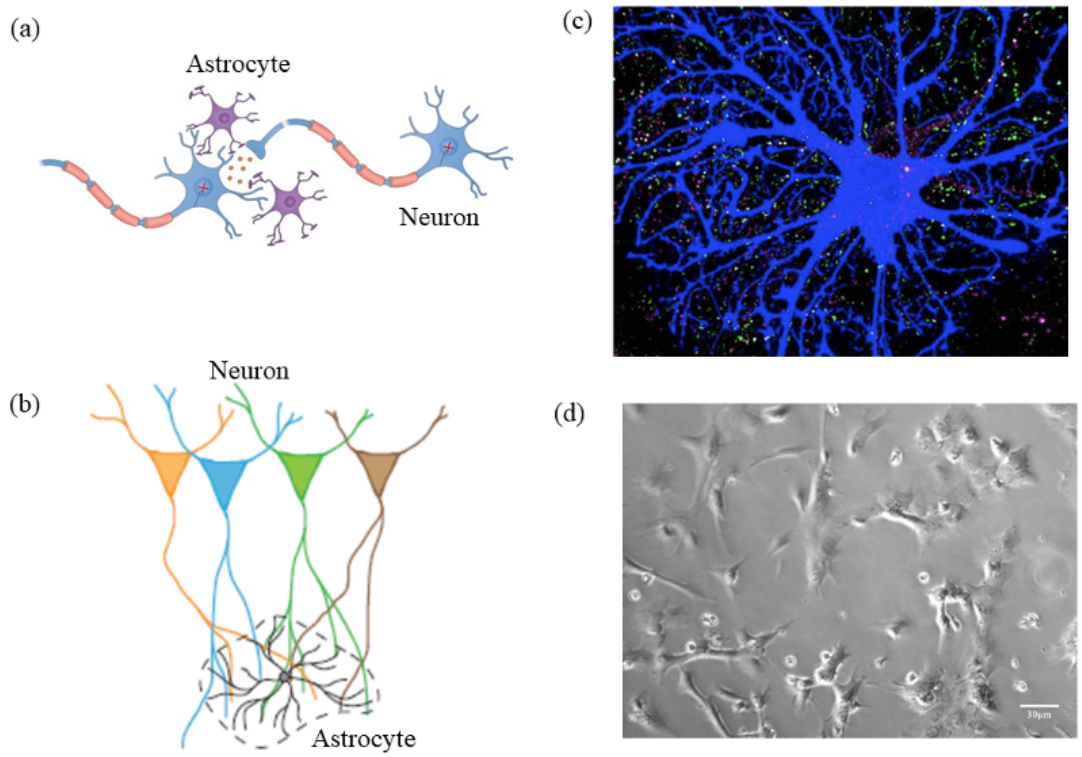

Figure 3.1: Astrocytes and their interaction with neurons. (a) Schematic representation of astrocytes in a neural network comprised of neurons. (b) Schematic representation of how a single astrocyte may modulate several synapses. (c) Fluorescence image showing a single astrocyte and the surrounding synapses (in green), from [43]. (d) Photograph of a culture of astrocytes on top of a glass (obtained in the laboratory of the group hosting this thesis).

Astrocytes can also form connections with neighbouring astrocytes through gap junction channels, creating a network that uses calcium to communicate (see figure 3.1). They also have sodium and potassium channels that create ionic currents, but unlike neurones, they do not generate or propagate APs. When internal or external stimuli activate these cells, they transmit specific instructions to adjacent cells, making it possible to consider them "excitable".

The gap junction channels referred to before are intercellular connections that enable the rapid exchange of ions and small molecules between adjacent cells. Connexins, a protein family abundant in astrocytes, form these channels to facilitate electrical and metabolic coupling. This connectivity supports functions such as energy supply to neurones, extracellular K+ and glutamate buffering, and calcium wave propagation [44]. Neuroactive substances modulate gap junctions, which are voltage-sensitive and allow their conductance to change with electrical potential differences between cells. Blocking these channels locally can reduce membrane voltage oscillations [45, 46].

Researchers have discovered that astrocytes play a role in the pathogenesis of several motor illnesses, such as Parkinson's disease [47, 48, 49], Alzheimer's

disease [50, 51], amyotrophic lateral sclerosis [52, 53], and Tourette's syndrome [54, 55].

3.2.2 Origins of Extracellular Signals

Extracellular signals refer to the electrical or ionic potential gradients generated on the cell membrane. These voltage gradients between cells arise due to the EFs, which are generated by the movement of ions and charged biomolecules across cell membranes [56]. Cell membranes not only have the ability to enclose the cell, but they also function as barriers, selectively determining what enters and exits the cell, thereby playing an important role in intercellular communication [57].

Small ions like protons, sodium, and potassium, as well as large molecules like tissue factors, growth hormones, neurotransmitters, and signaling molecules, form these gradients[56].

With all this information, it is possible to say that the source of extracellular signals relies on the structure and functions of the cell membrane, which are directly influenced by the EFs. Since this electric field depolarises and hyperpolarises the membrane potential, it triggers the expression of signalling factors that modulate processes like cellular regeneration and tissue remodelling[58].

It is important to mention that even in non-electrogenic cells, there are signals generated because of the ionic changes across the membrane, which contributes to the changes in membrane potential.

3.2.2.1 Equivalent circuit for the cell membrane

To better understand the concept of the cell membrane with ionic channels, electrical circuit models were implemented [59, 60]. Figure 3.2 illustrates the membrane equivalent circuit representing only one ionic channel, where the description of the behaviour of the membrane potential (V_M) and the movements of ions across the ion channels is given by electronic components.

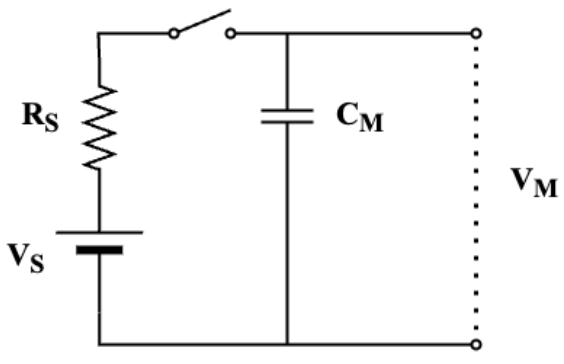

Figure 3.2: Equivalent circuit of the cell membrane

The electronic elements are a resistor R_S that represents the conductive pathway from the ion channel permeable to a specific ion species, in this study case is Calcium ions (Ca^{2+}); a battery source V_S that represents the ionic gradients; and a capacitor C_M that represents the membranes ability to store charge. A switch is also added to this circuit to consider the capacitor charges or discharges conditions, with the intuition of when the ion channel is close or open.

This circuit, in an electrical point of view, is a passive RC circuit, which means that it can only respond to an applied electrical signal. The term passive refers to the fact that neither the resistor nor the capacitor generates electrical signals on their own and remains unchanged regardless of the external stimulus.

3.2.3 Calcium waves/ions

Calcium signalling and the propagation of calcium waves characterise the distinct excitability of astrocytes.

Astrocytes have the ability to propagate increases in intracellular Ca^{2+} concentrations from a single cell to neighbouring cells, forming a wave-like pattern of communication. This type of signalling can occur spontaneously or in response to various external stimuli.

There are several ways that astrocyte Ca^{2+} signals come from inside the cell. These include pathways that involve different receptors, channels, exchangers, and pumps on the plasma membrane and in parts of the cell like the Golgi, mitochondria, and acidic organelles [61].

The membrane potential shifts generate weak and slow bioelectrical signals. These changes happen when charged ions move into or out of cells. This is closely connected to calcium waves. However, astrocytes have many ion channels that can also affect changes in membrane potential, such as Sodium ion (Na^+) channels [62].

3.3 Extracellular signal recording

3.3.1 Electrical equivalent circuit

Signals captured with microelectrodes *in vitro* (engl: in the glass) are known as extracellular signals. The microelectrodes are not implanted into the cell, hence avoiding any intrusion into the cell body. Therefore, they are classified as extracellular signals. The identification of these signals depends on the characteristics of the electrodes and the adherence of the cell membrane to the sending electrode, i.e., the coupling characteristics of the cell membrane to the electrodes.

The cells are placed in an electrolyte, and the areas between the cells and the electrode are covered with this electrolyte, which may be shown by an electrical equivalent circuit. These similar circuits facilitate understanding the coupling of charge fluctuations produced by a cell into the sensing electrode and their measurement as a voltage signal.

Figure 3.3 illustrates the equivalent circuit model representing the electrode/electrolyte interface with living cells adhered to the electrode's surface. This equivalent circuit illustrates the sensor that compromises two parallel electrodes, one of which acts as a measuring electrode and the other as a counter electrode. The electrical coupling of the extracellular signal to the sensing electrode, i.e., detection and capture of the signals generated by cells, and the electrode contribution to electrical noise, known as thermal noise, are determined by the impedance of these electrodes.

In the equivalent circuit, the extracellular signals in the equivalent circuit can be described by the electrical potential difference, $v_s(t)$, between the cells and the measuring electrode. This potential difference occurs because of the sum of all the currents originating from all the cells that cover the sensing structure.

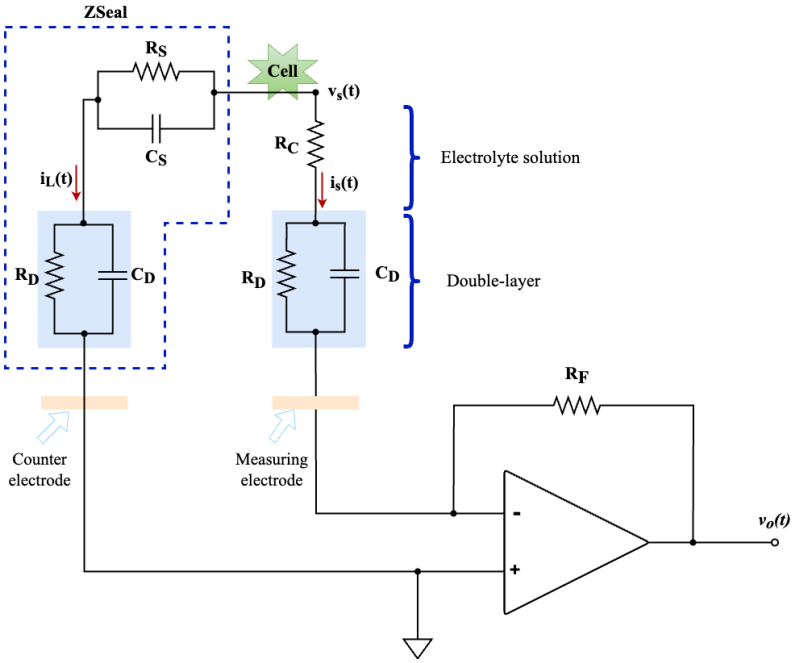

Figure 3.3: Schematic diagram of the equivalent circuit of the electrode/electrolyte interface.

As shown in Figure 3.3, this circuit is composed by several key components, so the electrical representation of the capture and amplification of the extracellular signal can be understood.

The resistance R_D and the capacitor C_D in parallel represent a simplified model of the EDL also known as Debye-Helmholtz layer, that is formed at the electrode/electrolyte interface, and it will be explained in mode detail in the following section.

The seal impedance (Z_{SEAL}) is usually defined as the impedance between the cell and the electrolyte, since is composed by the counter electrode double layer

impedance in series with the electrolyte impedance. The electrolyte impedance is illustrated by the resistance R_S in parallel with the capacitor C_S.

The spreading resistance, R_C, represents the signal loss between the cell and the measuring electrode, which only vailed when the cells are in contact with the sensing electrode. To have an effective recording of the extracellular signals, R_C needs to have a small value to ensure that the signal is coupled into the measuring electrode:

$$R_C << Z_{SEAL} \tag{3.1}$$

The amplifier shown in Figure 3.3 is a low-noise voltage preamplifier. The output voltage, $v_o(t)$, is the extracellular signal, $v_s(t)$, amplified and is given by:

$$v_o(t) = -R_F v_s(t) \tag{3.2}$$

where R_F is the feedback resistance, and $v_s(t)$ is the voltage at the terminals of the measuring electrode impedance.

It is important to mention that the current generated by the cells that flows through the Z_{SEAL} is represented by $i_L(t)$, and the current generated by the cells, which flows through the measuring electrode impedance, is represented by $i_s(t)$.

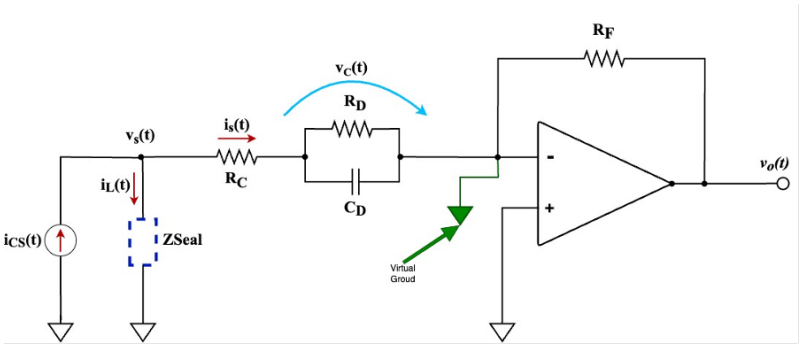

Figure 3.4: Simplified schematic diagram of the equivalent circuit illustrated in Fig.3.3.

To simplify understanding the equation that expresses the voltage across the EDL, a simplified schematic of the equivalent circuit is illustrated in Figure 3.4.

Given that the (-) input of the amplifier is a virtual ground, the following equation can describe the voltage $v_s(t)$:

$$v_s(t) = (\frac{v_c(t)}{R_D} + C_D \frac{dv_c(t)}{dt})R_C + v_c(t) \tag{3.3}$$

This equation can be rearranged to:

$$\frac{dv_c(t)}{dt} + \frac{(R_D + R_C)v_s(t)}{R_D R_C C_D} = \frac{v_s(t)}{R_C C_D} \tag{3.4}$$

Considering a particular solution of equation 3.4, when $v_s(t)$ is a voltage ramp increasing at a constant rate m, i.e., $m = dv_s(t)/dt$, then the solution of the equation 3.4 yields:

$$v_c(t) = k[t - \tau(1 - e^{-t/\tau})] \tag{3.5}$$

where,

$$k = \frac{R_D m}{R_D + R_C} \tag{3.6}$$

and,

$$\tau = \frac{R_D R_C C_D}{R_D + R_C} = C_D(R_C||R_D) \tag{3.7}$$

Here, τ is the time constant associated with the charging and discharging of the capacitor.

3.3.2 Electrical Double Layer (EDL)

As previously mentioned, the EDL is formed at the electrode/electrolyte interface, i.e., interface between a conductive material and an electrolyte medium. Initially, models of this layer were developed using aqueous solutions, but they were later extended to include ionic liquids and other electrolyte solutions [63]. The study of this interface is considered complex, both experimentally and theoretically [64]. For this reason, a simplified explanation of the EDL will be given. This layer forms when two phases with different electrochemical properties come into contact, leading to a redistribution of charge and potential at the boundary. This process persists until the electrochemical potentials of the charge carriers in both phases are the same, i.e., they reach equilibrium [65].

The EDL acts as a dipole layer, consisting of ions on the electrolyte side and electrons on the electrode side. The layer is only a few nanometres thick. The high concentration of ions near the electrode's surface arises from their attraction to counterbalance the electrode's typically negative charge. Further from the electrode, the ion concentration gradually decreases until it reaches the bulk concentrationthe equilibrium level of ions in the electrolytewhere the electrode's influence no longer affects the ions [66].

The EDL consists of two distinct layers: Stern layer and Gouy-Chapman layer [63].

The Stern layer, also referred to as the Helmholtz layer, is the region closest to the electrode's surface, where an accumulation of counterionstypically positive ionsoccurs due to strong electrostatic attraction from the charged electrode,

typically negative. Because these ions are tightly connected and cannot move freely, they form a compact layer that partially neutralises the electrode's surface charge. The Stern layer has behaviour similar to a capacitor, as the tightly bound ions create a charge layer that closely balances the electrode's charge.

The Gouy-Chapman layer, also known as the Diffusive layer, is a diffuse layer that extends outward from the Stern layer into the electrolyte solution. The ions in this region exhibit a more loose distribution, allowing them to move freely and without tight connections. The concentration of ions gradually decreases as the distance from the electrode rises. This layer represents a balance between the electrostatic attraction pulling ions towards the electrode and the thermal motion that disperses them.

3.3.2.1 Circuit model

An equivalent circuit model, also known as the Radels and Somerton model, of the electrode-electrolyte interface is shown in Figure 3.5 to provide a better perspective of this interface [67].

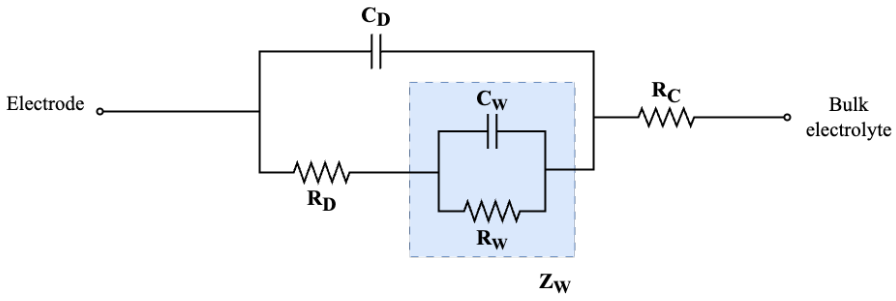

Figure 3.5: Equivalent circuit model of the electrode/electrolyte interface.

This circuit model includes the EDL capacitance (C_D) in parallel with the EDL resistance (R_D) and with the Warburg element (Z_W).

In this model, the Warburg element (Z_W) is represented as a parallel RC circuit combination between R_W and C_W. This element impedance is caused by the ions diffusion, i.e., the ions slow movement through the electrolyte in the direction of the electrode. However, the contribution of the Warburg components to the recording of extracellular signals is lower compared to the contribution of the other elements, allowing their removal and hence simplifying the equivalent circuit model [68].

The spreading resistance (R_C) represents the electrolyte resistance, also known as the "bulk" solution resistance. R_C is the resistance encountered by current spreading out from the sensing electrode into the counter electrode through the electrolyte. The electrode's surface geometry determines this resistance.

3.4 Noise

Noise refers to unwanted electrical impulses that have the potential to modify the measured signal. The noise could be insignificant if the prediction of the instaneous amplitude of noise was possible [69].

One challenge in monitoring low-frequency extracellular bioelectrical activity is that the target signals are often weak and easily masked by both external and internal sources of noise. To combat this challenge, the method recommended by [7] will be used, with some modifications, to properly evaluate these signals while minimising the influence of noise.

This method consists of measuring weak and low-frequency biological signals using extracellular electrodes. This approach takes advantage of the Helmholtz capacitive double-layer that was explained in Section before. This is achieved by measuring the displacement current that flows through the double-layer capacitor as a result of the small extracellular voltage fluctuation, which is measured in the order of V (micro-volts).

The proposed of this method is to measure low-frequency neural oscillations, such as signals generated by astrocytes, which play an important role in brain functions and have been associated with brain disorders, using extracellular electrodes.

To give the reader a better understanding of this method, there was a discussion and presentation of the equivalent circuit used to describe the electrical coupling between the cell and the sensing electrode in Section 3.3. In the following section, it will be explained the noise evaluation based on this method.

3.4.1 Analysis of noise evaluation

The noise contributed by the electrodes depends on the noise they generate and how effectively this noise is coupled to the front-end amplifier.

In [7], the authors evaluate the electrode impedance (capacitance and resistence) and their frequency dependence to understand how the electrodes contribute to the system noise. They simplified the circuit, without cells, of the high-impedance double layers in series with the low-impedance double layer (Figure 3.3) to an equivalent RC network, discribed by R_s and the capacitance C_s. This RC network is schematically represented in Figure 3.6.

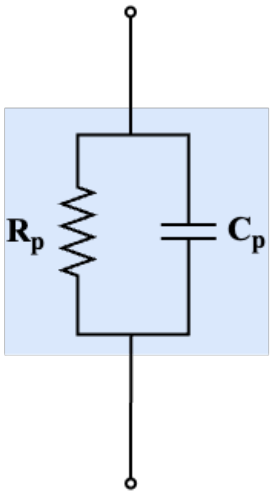

Figure 3.6: Equivalent RC network of the high-impedance double layers in series with the low-impedance double layer.

The equivalent admittance Y_T of the R_s in parallel with C_s is given by:

$$Y_T = \frac{1}{R_p} + j\omega C_p \tag{3.8}$$

where R_p is the total parallel resistance and the C_p is the total parallel capacitance.

The total parallel resistance is described by:

$$R_p(\omega) = \frac{(R_D + R_S)^2 + \omega^2 R_D^2 R_S^2 (C_D + C_S)^2}{R_D + R_S + \omega^2 R_S R_D \left(R_D C_D^2 + R_S C_D^2\right)} \tag{3.9}$$

and the total parallel capacitance is expressed as:

$$C_p(\omega) = \frac{R_D^2 C_D + R_S^2 C_S + \omega^2 R_D^2 R_S^2 C_D C_S (C_D + C_S)}{(R_D + R_S)^2 + \omega^2 R_D^2 R_S^2 (C_D + C_S)^2} \tag{3.10}$$

Ultimately, they determined that the noise generated by the electrode arises resistance, R_p, indicating that this noise exhibits a considerable dependence on frequency. This phenomenon is commonly referred to as thermal noise.

In the upcoming sections, a brief description of thermal noise and $1/f$ noise will be provided, since these types of noise will be mentioned throughout this work.

3.4.2 Thermal noise

Thermal noise was first detected by J.B. Johnson in 1927 [70], followed by a theoretical analysis by H. Nyquist in 1928 [71]. Hence, this phenomenon is also

referred to as Johnson noise or Nyquist noise.

This noise originates from the random thermally induced vibrations in the charge carriers of any material with a finite resistivity, specifically from the thermal instabilities of the electrons. Even though the average movement of these carriers is zero, the instantaneous random motion of the electrons creates instantaneous charge gradients. These gradients lead to wide-band random voltage fluctuations, thereby creating a voltage across the conductor.

This noise can be modelled mathematically as an ergodic Gaussian random process, representing random fluctuations in charge carriers within a material. Figure 3.7 shows the simplified representation of this process by using an equivalent voltage source, v_n, in series with a noise-free resistor [69, 72].

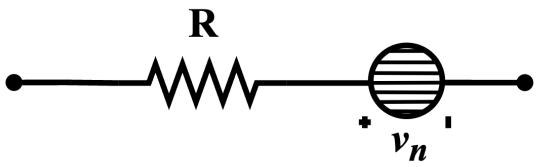

Figure 3.7: Equivalent voltage source in series with a noise-free resistor

Experimental studies have shown that the intrinsic noise of any circuit element is basically thermal [73], following the standard Johnson noise equation that quantifies the root mean square (RMS) voltage noise of a resistance at room temperature as:

$$v_{\text{rms}} = \sqrt{\int_{f_1}^{f_2} 4kTR(f)\,df} = \sqrt{4kTR\Delta f} \tag{3.11}$$

where k is Boltzmann's constant, T is the absolute temperature in Kelvin (K), Δf is the bandwidth of interest ($f_2 - f_1$) in Hertz (Hz), and R is the resistance or the real part of the conductors impedance in Ohms (Ω).

One of the most relevant features of thermal noise is its independence with frequency, since the Power Spectral Density (PSD) for thermal noise is constant from DC to frequencies up to near infrared and can be considered as white noise [72], i.e., the noise is constant across all frequencies.

For spectral analysis of the electrode noise, equation 3.11 can be expressed in terms of their PSD functions as:

$$S_V \equiv \frac{\langle v_n \rangle^2}{\Delta f} = 4kTR\,(\text{V}^2/\text{Hz}) \tag{3.12}$$

where S_V represents the voltage noise PSD function and the term $\langle v_n \rangle^2$ represents the square average of the voltage noise source.

Thermal noise is considered the fundamental noise level in any electrical system, as thermodynamic equilibrium is unavoidable in most cases. Other sources of noise in an electrical system, such as 1/f noise discussed below, are classified as excess noise.

3.4.3 Flicker noise ($1/f$ noise)

The $1/f$ noise, also known as flicker noise, consists of the exhibition of an unpredictable increase without limits as the frequency decreases in the spectral density of a population of data. Many fields, including acoustics, physics, biology, economics, construction, and most likely others, have discussed this phenomenon [74, 75, 76, 77, 78, 79, 80].

The name of this noise arises from the observation, in datasets from various systems or even those gathered from identical systems, that the increase in spectral density as frequency decreases follows a $1/f_\alpha$ pattern, with the exponent α typically reported as unitary ($\alpha = 1$), although it has also been documented to range from 0.5 to 2 ($0.5 \leq \alpha \leq 2$).

Until now, it was not proposed a unified theoretical explanation that defines $1/f$ noise, and its physical origins remain unsolved [74, 69]. For this reason, this phenomenon is referred to in literature by various names, such as flicker effect (or flicker noise), semiconductor noise, low-frequency noise, pink noise, current noise, and contact noise. However, the literature has proposed some empirical and theoretical models based on results from experimental measurements [69, 76, 81].

In this document, the discussion of this noise will focus on the increase in noise levels commonly seen in electrical systems as the frequency decreases.

One of the empirical models that, even after being submitted to several revisions and experiments by many scientists, is still valid and adapted to describe the spectral density of $1/f$ noise is the model presented by Hooge [82]. Interestingly, while Hooge's model primarily accounts for the passage of a direct time-invariant current (I_{DC}) through the electrical system, it has not been refuted in situations where no current is applied, suggesting its broader applicability. The result for determining the voltage spectral density of $1/f$ noise ($S_{1/f}$), as proposed by Hooge for homogeneous samples, is given by:

$$\frac{S_{1/f}}{\langle v_{n,1/f} \rangle^2} = \frac{K}{f^\alpha} \tag{3.13}$$

where K is a constant unique to a particular electrical system proportional to the rate between the Hooges parameter (aH) and the number of charge carriers (NC), f is the frequency, the exponent is a constant, typically in the range of 0.5 to 2, depending on the properties of the electrical systems, and the terms $\langle v_{n,1/f} \rangle^2$ refer to the mean square of the voltage noise sources.

Although the estimation of the spectral density of $1/f$ noise is based on an empirical model, it is possible to determine the noise content in a frequency band by integration over the range of frequencies in which this thesis' interest lies. This is feasible because the $1/f$ noise is inversely proportional to frequency and because of the consideration that $1/f$ noise is a stochastic process modelled by a zero-mean ergodic Gaussian. The total noise power (P_n) considered for a frequency band (Δf) can be calculated as:

$$P_n = \int_{f_L}^{f_U} \frac{K}{f} df = K \ln\left(\frac{f_U}{f_L}\right) \tag{3.14}$$

where both P_n and K have units in watts (W), and f_U and f_L are the upper and lower frequency limits of the Δf being considered. Equation 3.14 shows that the noise power depends on the logarithmical ratio of the upper and lower frequency bounds. It is notable that, for any decade in frequency ($f_U = 10 f_L$, P_n), P_n ramains constant and is given by $\boldsymbol{K \ln 10}$. This arises because the logarithmic term simplifies to ln 10, leading to a constant P_n contribution across any frequency decade. As a result, $1/f$ noise contributes an equal amount of power per frequency decade, and, since the $1/f$ noise is uncorrelated across different frequency ranges, the P_n increases as the square root of the number of frequency decades.

Moreover, increasing the length of the measuring time does not improve the measuring accuracy while considering $1/f$ noise. In contrast, when measuring white noise, such as thermal noise, the accuracy increases as the square root of the measuring time.

3.5 Conclusion

This chapter tries to provide a concise review of the concepts and methods used throughout this thesis. These concepts focus on providing a biological context, clarifying the extracellular signal capture process, and explaining the electrode's noise, which contributes to the overall system noise.

Chapter 4

Methods and Materials

This chapter mentions the electrophysiological sensing structures used to record the extracellular signals. Firstly, a brief explanation of the sensing electrodes used in this study and the IT device sample holder fabricated to hold a set of electrodes is given. The setup of the instrumentation used to record extracellular bioelectrical activity using computer-base processing techniques is explained. Finally, a brief mention of the biological material is provided.

4.1 Sensing structures

The purpose of sensing structures, often referred to as electrodes, is to establish a physical link between two surfaces, which allows the acquisition of signals generated by cells in extracellular communications, i.e., the signal originated from one interface is transformed into an equivalent signal with the mobility properties of the other interface. The fabrication and design of these devices must meet specific parameters, such as incorporating a layer that promotes cell adhesion to the electrode and using electrodes with low-impedance. To achieve these specifications, researchers optimise the dimensions and geometry of the electrodes. In this thesis, the electrodes are transduction devices based on plain surfaces. Typically, glass and polymers are used as materials to create the electrodes' base surfaces.

This dissertation employed two distinct types of devices. The first type is the commercial 8 Well PET arrays, manufactured by Applied Biophysics in New York, USA. The arrays consist of gold electrodes based on polyethylene terephthalate (PET) substrate. The second type was designed by the team hosting this thesis. This device consists of five distinct circular gold electrodes of different widths and a centre round electrode with a diameter of 60 micrometres (μm). The round electrode is coated with a layer of Graphene Oxide (GO). The electrodes are based on either glass or Silicon Dioxide (SiO_2).

Two chapters of this thesis will provide a thorough description of each device. These chapters conduct studies to emphasise the role of electrodes in capturing intercellular interactions.

4.1.1 IT devices sample holder

In this thesis, some experiments will use the device sample holder developed by the group hosting this thesis, which can be seen in figure 4.1. This holder's design necessitated its mounting in a sandwich-like configuration. Each holder is composed of two laser-cut components fabricated from 3 millimetres (mm) thick transparent poly(methyl methacrylate) acid (PMMA). The upper portion of these pieces served as a supporting layer. On the contrary, the piece on the bottom was used to compress the sealing layer, a 35 mm diameter petri dish. Four pairs of stainless steel screws and nuts were used to attach the bioelectronic electrode of this experiment to the sample holder.

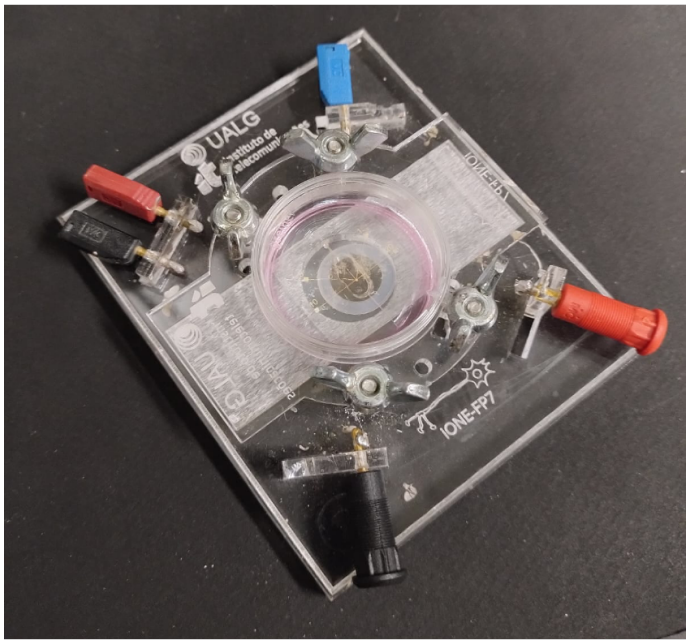

Figure 4.1: Photograph of the IT devices sample holder.

4.2 Instrumentation

The instrumentation used in the studies conducted for this thesis centres on recording extracellular communications between cells, facilitated by specific software and hardware.

4.2.1 Setup for the experimental recordings

The experimental set-up includes a signal acquisition system designed for recording ultra-weak signals from non-electrogenic cells.

Figure 4.2 shows that the system consists of a low-noise voltage preamplifier directly coupled to the transducer device within a die-cast aluminium case. After the amplification of the signals, they can be detected by the digital signal analyser, where the time scale is carefully adjusted to capture the nuances of the signal. The digital signal analyser then transfers the signals to the PC for further processing.

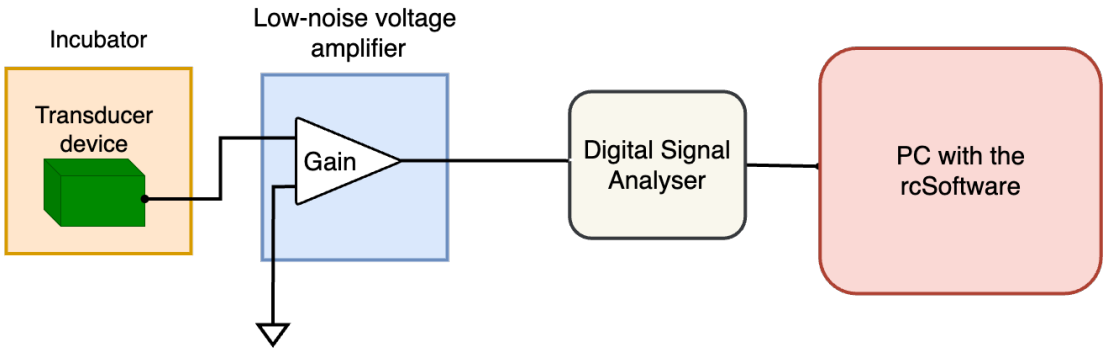

Figure 4.2: Schematic diagram of the signal acquisition system

The real acquisition signals system components are shown in Figure 4.3, which consists of a commercial low-noise voltage preamplifier, SR560 low-noise amplifier (LNA)[83], produced by Stanford Research Systems, Sunnyvale, California, USA, connected to a die-cast aluminium case containing the transducer device. The SR560 LNA was coupled to an Agilent 35670A Fast-Fourier Transform (FFT) Digital Signal Analyser (DSA) using a 0.5 meter low-noise coaxial cable. The DSA is now held by Keysight Technologies in Santa Rosa, USA [84]. The acquired data is then transmitted to the PC using the rcSoftware shown in Figure 4.4c. The group hosting this thesis developed this software particularly for signal acquisition, collection, and processing for this type of system [85].

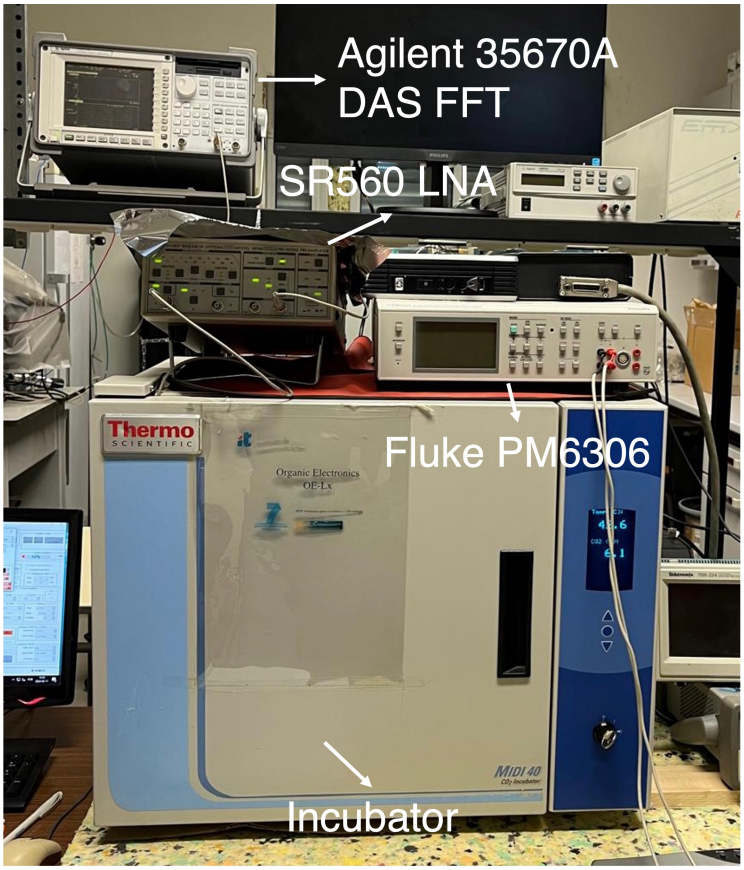

Figure 4.3: Photograph of the signal acquisition system

The transducer device is contained inside a die-cast aluminium case, as seen in Figure 4.4a) and Figure 4.4b). The die-cast aluminium case has a Bayonet-Neill-Concelman (BNC) connection for connecting the transducer device to the SR560 low-noise amplifier LNA via a 1 meter low-noise coaxial cable. The case is then positioned into an incubator to preserve optimal conditions for the cells, hence ensuring that the findings remain unaffected by external variables.

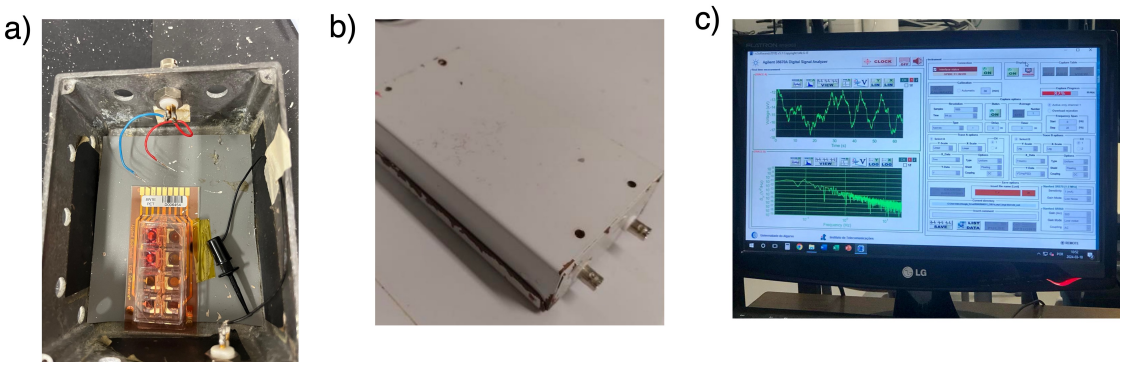

Figure 4.4: Other components that are part of the experimental set-up system. a) Die-cast aluminium case with transducer device. b) Die-cast aluminium closed c) PC using rcSoftware

Before placing the transducer device inside the cast, the electrodes are connected to the measuring device using gold wires secured with liquid silver. Both materials are extremely conductive.

An impedance analyser, Fluke PM6306 (Fluke Corporation, Everett, USA), was used to verify if the gold wires were connected correctly and to measure small signal impedance. A self-developed software named RCL, compatible only with Microsoft systems, was used to remotely manage and perform all measurements in this study [86, 87].

To protect the recording system from electromagnetic interference, the system was positioned on top of anti-vibrational mounts.

4.3 Biological material

Astrocytes (C8-D1a) were used in this study and were purchased from the America Type Culture Collection (ATCC) Organisation, Manassas, Virginia, USA [88].

C8-D1a were maintained in culture with Dulbecco's Modified Eagle's Medium (DMEM) with high glucose content and Neurobasal medium, supplemented with 10% (v/v) heat-inactivated foetal bovine serum (FBS), 1% (v/v) penicillin-streptomycin antibiotic solution, and 1% (v/v) Amphotericin-B fungicide solution (Sigma-Aldrich, Missouri, USA). The culture was incubated at 37 °C in a humidified atmosphere with 5% Carbon dioxide (CO_2) (Thermo Fisher Scientific, New York, USA).

Aliana Vairinhos and Dr. Rute Félix were the only ones responsible for caring for, handling, and preparing cell cultures for experiments.

4.4 Conclusion

This chapter explained the methods and experimental setup used to achieve a precise record of extracellular bioelectrical activity. The first part of the chapter focuses mainly on the sensing electrodes and the instrumentation used for this type of recording. The chapter concludes with a brief discussion of the astrocytes used and their maintenance.

Chapter 5

Study of bioelectrical signals

This section focus on the explanation of the biological signals that will be encounter along the experiences made. This explanation will count with the following structure: it first be present the different types of signals by describing their evolution, then it will be explained and calculated the power of a typical signal that occurs in this study.

5.1 Introduction

Over the years, numerous fields of science have intensively researched different types of signals. The objective of this study is to get a comprehensive understanding and increase familiarity with the extracellular signals produced by astrocytes, since this topic is currently lacking information in the existing literature.

Bioelectrical signals refer to the collective set of signals produced by cells, tissues, and organs. The majority of these signals are action potentials (APs), which are electrical signals produced by the mechanical contraction of a single cell when activated by an electrical current that may originate from inside or outside the human body [89, 90].

A concise literature overview of various bioelectrical signals is provided in table 5.1. This table displays a variety of bioelectrical signals along with their relevant features, including their origins, typical frequency, and amplitude range.

Table 5.1: Different types of bioelectrical signals and their characteristics[90, 89, 91].

Bioelectrical Signal	**Signal Origin**	**Frequency (Hertz (Hz))**	**Amplitude (millivolts (mV))**
Electrocardiogram (ECG)	APs of Heart muscle cells	0.05–250	0.01–5
Vectorcardiogram (VCG)	APs of heart muscle cells	0.05–150	0.01–2
Fetal ECG (fECG)	Fetal heart activity	0.05–250	0.01–0.02
Electroencephalogram (EEG)	Brain neurons activity	0.1–80	0.005–0.3
Evoked Potentials (EP)	Brain activity in reaction on external stimuli	30–3000	0.0001–0.02
Electrocorticogram (ECoG)	Signal generated by cerebral cortex	0.1–100	0.005–10
Electroneurogram (ENG)	APs of peripheral nerves	0.01–1000	0.005–10
Electromyogram (EMG)	APs of muscle fibbers	0.01–10,000	0.1–10
Electrogastrogram (EGG)	Gastric muscles activity	0.02–0.15	0.01–0.5
Electrooculography (EOG)	Stiff muscles activity	0.5–15	0.05–3.5
Electroretinography (ERG)	Eye retina activity	0.2–50	0.005–1
Electrohysterography (EHG)	Uterus activity during contractions	0.1–3	0.1–5
Phonocardiogram (PCG)	Signal of the sound produced by the contractile activity of the heart and blood together	————————	————————

The research on signals produced by brain cells, such as EEG signals, has mostly focused on recording neuronal signals, therefore reinforcing the clearly evident knowledge gap between neurons and astrocytes.

In this study, every type of signal acquired from the recordings of astrocytes will be reported. Further, an analysis of the signal power will be conducted to enhance comprehension of these results.

5.2 Types of signals

Upon analysing signals acquired using the materials and methods outlined in Chapter 4, a variety of signals were identified, since it is hypothesised that signals experience changes based on their amplitude. When the signal ampli-

tude increases significantly, the biphasic signal exhibits symmetry. Additionally, monophasic and biphasic signals with the same features are not distinct. One notable feature is that the biphasic signals often exhibit a down-up; however, sometimes they are up-down.

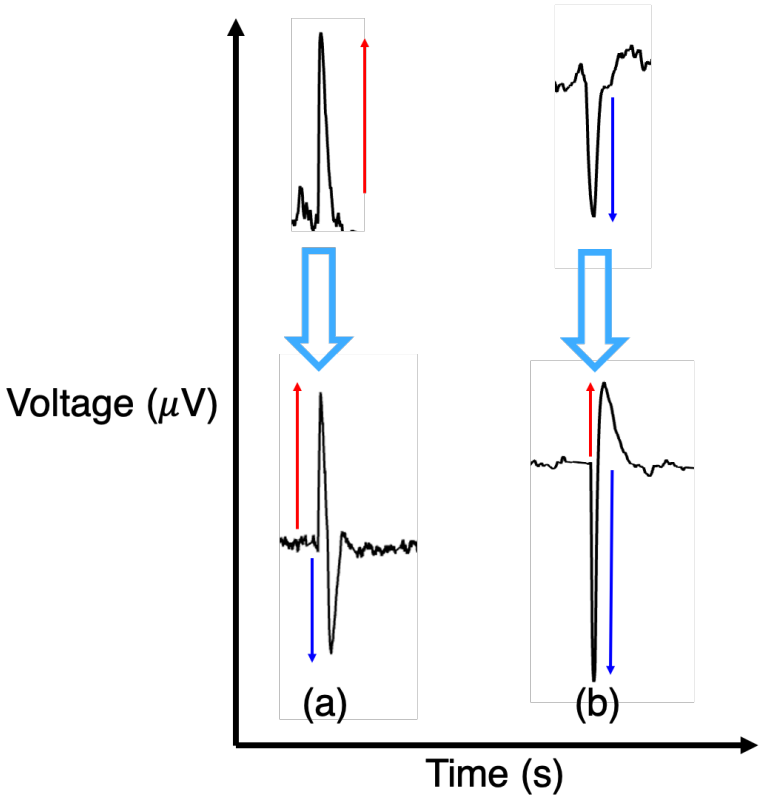

Figure 5.1: (a) Evolution of a monophasic signal up to a biphasic signal up-down. (b) Evolution of a monophasic signal down to a biphasic signal down-up.)

Biphasic signals are characterised by a waveform that shows two different phases, normally a rapid depolarisation followed by a repolarisation (down-up), as can be seen in figure 5.1. However, these signal phases can also be a rapid repolarisation followed by a depolarisation (up-down).

Among these signals, it was observed that the biphasic signals, particularly the down-up signals, occur more frequently and contain more information about the functions and behaviours of astrocytes.

The following section will be dedicated to the signal power of a typical biphasic signal with the objective of finding the typical order of magnitude of the signal power.

5.3 Signal Power

The signal power in chapter **??** was obtained by calculating the area under the signal, which in a way is proportional to the power because it is the volts in a time interval.

To understand better the results obtained in chapter **??** and how the signal power calculation is proportional to the area under the signal, it was created an equivalent sinusoidal wave of a typical biphasic signal of this study.

The equivalent signal is defined by the equation:

$$x(t) = A \sin\left(2\pi \frac{1}{T} t\right) \tag{5.1}$$

where A is the typical amplitude of study signals and T is the duration of the signal.

Next, a brief deduction of the power equation is given followed by a explanation of the MATLAB implementation and the results obtain from it.

5.3.1 Theoretical explanation

According to [92], the power of the signal, also known as average power [93], can be obtained from:

$$P_x = \lim_{T\to\infty} \frac{1}{T} \int_{-\frac{T}{2}}^{+\frac{T}{2}} |x(t)|^2 \, dt \tag{5.2}$$

By substituting $x^2(t) = A^2 sin^2\left(2\pi \frac{1}{T} t\right)$ and knowing that $\sin^2(\phi) = \frac{1}{2}(1 - \cos(2\phi))$, $x^2(t)$ can be equated as:

$$x^2(t) = \frac{A^2}{2} - \frac{A^2}{2} \cos\left(4\pi \frac{1}{T} t\right) \tag{5.3}$$

As a result, by substituting $x2(t)$ in equation 5.2, the power is as follows:

$$P_x = \lim_{T\to\infty} \frac{1}{T} \int_{-\frac{T}{2}}^{+\frac{T}{2}} \left(\frac{A^2}{2} - \frac{A^2}{2} \cos\left(4\pi \frac{1}{T} t\right)\right) \, dt \tag{5.4}$$

Splitting the terms in equation 5.4:

$$P_x = \lim_{T\to\infty} \frac{1}{T} \int_{-T/2}^{T/2} \frac{A^2}{2} \, dt - \lim_{T\to\infty} \frac{1}{T} \int_{-T/2}^{T/2} \frac{A^2}{2} \cos(4\pi f t) \, dt \tag{5.5}$$

The second limit in equation 5.5 is equal to zero (0) because the integral of a periodic function over a long period of time tends to zero (0) as the positive and negative oscillations cancel each other.

On the other hand, the first limit is:

$$\lim_{T\to\infty} \frac{1}{T} \cdot \frac{A^2}{2} \int_{-T/2}^{T/2} 1\, dt = \lim_{T\to\infty} \frac{1}{T} \cdot \frac{A^2}{2} \cdot T = \frac{A^2}{2} \tag{5.6}$$

Therefore, the power of the signal for this equivalent signal is equal to:

$$P_x = \frac{A^2}{2} \tag{5.7}$$

In order to obtain satisfactory results, the power will be calculated in two ways.

5.3.2 MATLAB implementation and results

Initially, the equivalent sinusoidal wave was implemented in a script using MATLAB, where A is the typical amplitude of study signals with a value of 94 microvolts (μV) and T is the period of the sinusoid with a value of 48 seconds.

Then, the power was calculated using the equation 5.5 and using an adapted version of the equation 5.2. This adapted version gives the average power of the equivalent signal over the period of time T and can be defined by:

$$P_x = \frac{1}{T} \int_0^T |x(t)|^2\, dt \tag{5.8}$$

To implement the equation 5.8 on MATLAB, it was used the function `trapz` to calculate the integral of $x^2(t)$. This function applies the **trapezoidal rule**, which is the sum of the areas of the trapezoids formed by the sampled points of the signal along the interval [0,T] [94].

Both methods provide the same value, which increases the credibility of the result and permits the confirmation that the order of magnitude of the power of the typical signals in this study is 10^{-9}(nano).

5.4 Conclusion

The chapter explores the variety and complexity of bioelectrical signals. Initially, the chapter provided an overview of various bioelectrical signals, including their origins, frequency ranges, and amplitudes. The aim of this overview was to demonstrate the lack of information about signals generated by astrocytes compared to others.

The possibility of an evolution of the signal generated by astrocytes was presented, where the forms of it went from monophasic to biphasic forms. This evaluation was analysed in relation to their amplitude and symmetry, which allowed the hypothesis that these signals change based on their amplitude.

In order to extract an additional characteristic of these typical signals, an equivalent signal was implemented. This signal, a sinusoid wave with the amplitude of a typical signal from this study, is designed to simplify the calculation of the signal's power. The power was calculated through a MATLAB scrip in two ways. Both ways gave the same results, which establishes that the typical order of magnitude of astrocytic signals is at the scale of $10^{-}9$ (nano).

Hence, this chapter provides new information and narrows the existing gap of knowledge in astrocytes' signals.

Chapter 6

Impact of the sensing electrode design and geometry on signals power

6.1 Introduction

In biological systems, the sensing electrodes play an essential role in the recording and interpretation of electrical signals generated by cells. In particular, astrocyte populations are believed to cooperate and synchronise their activity, thus producing waves that propagate across tissues or compact cell monolayers. These waves are commonly referred to as calcium waves [95, 96, 97, 98].

Even though calcium oscillations occur within astrocytes, they may also produce an extracellular component that can be detected by external electrodes. Calcium waves typically propagate at speeds of 10-50 micrometres per second ($\mu m\ s^{-1}$) [99]. Calcium fluorescence probes are typically used to visualise the calcium waves in the optical microscope. However, a work hypothesis was formulated to understand how extracellular electrodes can electrically detect calcium waves instead of using optical methods.

A detailed explanation of this work hypothesis will be provided in Section 6.1.1.

This chapter presents two devices with a variety of electrode designs and the analysis of the corresponding extracellular signal recordings. This analysis focuses on choosing discrete signals with well-defined shapes to acquire a precise calculation of their area.

6.1.1 Working hypothesis

Comentário: Não sei se a hispotese de trabalho continua ou não.

The aim of this analysis was to comprehend the impact of electrode design and dimensions on results obtained from their use. It was theorised that these design factors, specifically the dimensions, have a significant impact on the char-

acteristics of the signals collected, with a specific focus on differentiating between measurements of cell synchronisation and travelling waves.

To give a better understanding of the concept of using electrodes to detect travelling waves, this was illustrated in Figure 6.1.

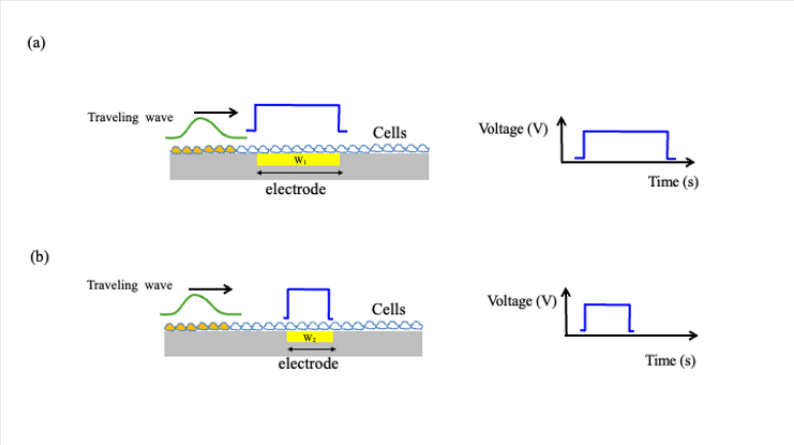

Figure 6.1: Conceptual view of recording a travelling wave using extracellular electrodes. (a) A wave crossing an electrode with width W1. (b) A wave crossing a shorter electrode with width W2.

To achieve clarity on this matter, electrodes of different dimensions were created and implemented. The working hypothesis suggests that the surface area of the electrode has a direct influence on the signal area of the detected signals. As a result, the concept of a theoretical maximum synchronisation length for cell clusters was introduced. The extent of the electrode's coverage would determine this length. Contrary to initial predictions, the size of the electrodes did not offer conclusive proof of their capacity to measure travelling waves. However, the data indicated a pattern of signal distribution that is more closely aligned with cell synchronisation phenomena. Specifically, it was noted that smaller electrodes could potentially enhance the signal distribution by increasing the probability of synchronising all cell clusters within their range.

The observed patterns of signal distribution provided evidence in favour of the cell recruitment model. Based on this model, the synchronisation of cell clusters is made easier by travelling waves. The duration of the signals corresponds to the time it takes for the waves to travel over the electrodes. Interestingly, the size of the electrode seemed to impact the selection of cell clusters, as larger electrodes were able to capture a wider range of signals by covering a greater number of clusters. Therefore, the investigation emphasised that the size of the electrodes significantly influences the characteristics of the signals detected, which supports the cell recruitment model as opposed to direct wave measurement. This discovery presents new opportunities for further study, specifically in examining the effects of electrode size on the precision and distribution of signals for better

measurements.

6.2 Experimental

Astrocytes cells were measured using the setup for recording ultra-weak extracellular signals presented in Chapter 4. These cell measurements only took place when a confluent monolayer was reached.

6.2.1 Sensing structures

The sensing structures, also known as sensing electrodes, used to capture the bioelectrical activity of the astrocytes' populations in this study will be described to give the reader a better understanding of how they work. This experiment used two types of electrodes: (a) a commercial 8-Well PET array (IBIDI device) and (b) circular electrodes.

(a) Commercial 8 Well PET Array (IBIDI device)

The configuration of the commercial 8-Well PET array used was the 8W1E PET, and it was purchased from IBIDI. Unfortunately, this manufacturer has stopped fabricating these devices, and they are no longer available for consultation on the website. However, since Applied Biophysics is the source of these devices, their website will be used as a reference [100].

The 8W1E PET device consists of 8 well PET arrays organised in a pattern of gold electrodes per well on a polyethylene terephthalate (PET) substrate. These wells consist of only one round electrode with a diameter of 250 micrometres (μm), resulting in a minimum area of 0.00049 glscm. The total area of these electrodes may be adjusted by the specific amount of Sodium hydroxide (NaOH) applied. This is possible due to the presence of a polymer layer that, when combined with NaOH, permits the investigation of a variety of electrode areas. Additionally, a thin layer of curried photoresist polymer is used to separate the gold tracks located between the electrodes and larger contact pads.

The 8W1E PET IBIDI device configuration is shown in figure 6.2(a), which is a scaled version of the original size. The open gold is shown by yellow areas, and the cured photoresist polymer layers are shown by orange areas. The layout of the electrode in this device is illustrated in figure 6.2(b). Figure 6.2(c) shows a photo of the 8W1E PET device used in this experiment.

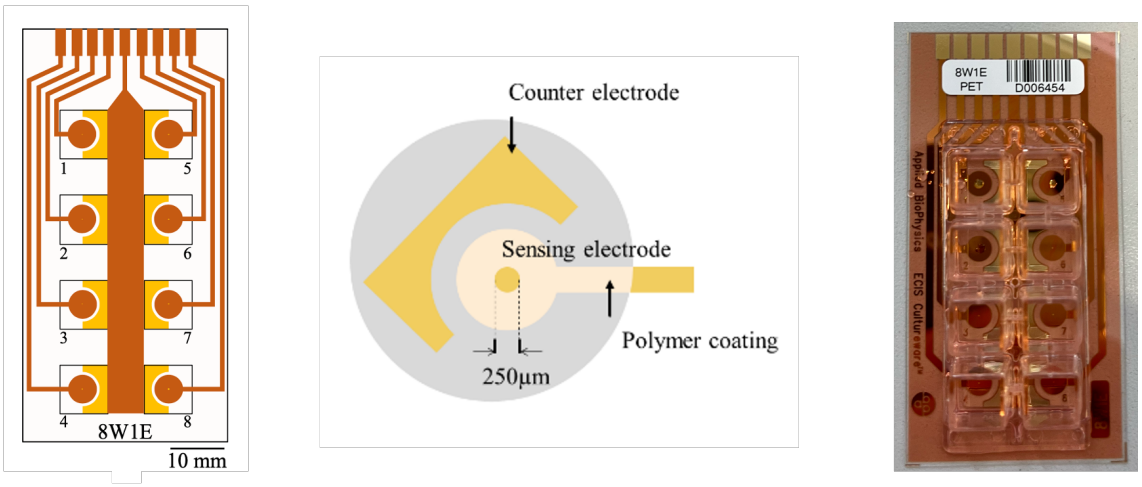

Figure 6.2: (a) IBIDI device, with the 8W1E PET configuration, scaled to their original dimensions. (b) Detailed view of the electrode layout. (c) Photo of the 8W1E PET array sample.

(b) Circular electrodes

Figure 6.3(a) displays a photograph of the complete electrode array that was fabricated on a Silicon Dioxide (SiO_2) substrate. This experiment used five independent gold electrodes with a circular pattern, each with a defined width. The particular width of each electrode can be seen in detail in figure 6.3(b) These gold electrodes were produced by thermal evaporation and lithography on top of the SiO_2 substrate.

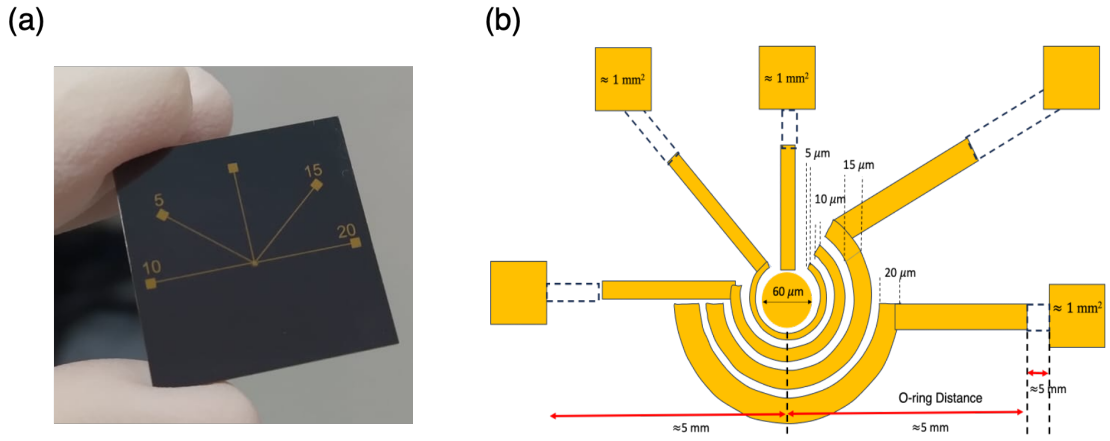

Figure 6.3: (a) Photo of the entire electrode array. (b) layout of the entire electrode array.

6.2.2 Methodology

As studied in Chapter 5, the electrical signals recorded from the cultured astrocytes that interface with microelectrode arrays can be categorised into three different types: monophasic up signals, monophasic down signals, and biphasic signals.

To enhance the evaluation of the effect of the geometry and electrode surface area, the selected signals for this study were the biphasic signals (Figure 6.4(a)) and monophasic up signals (Figure 6.4(b)).

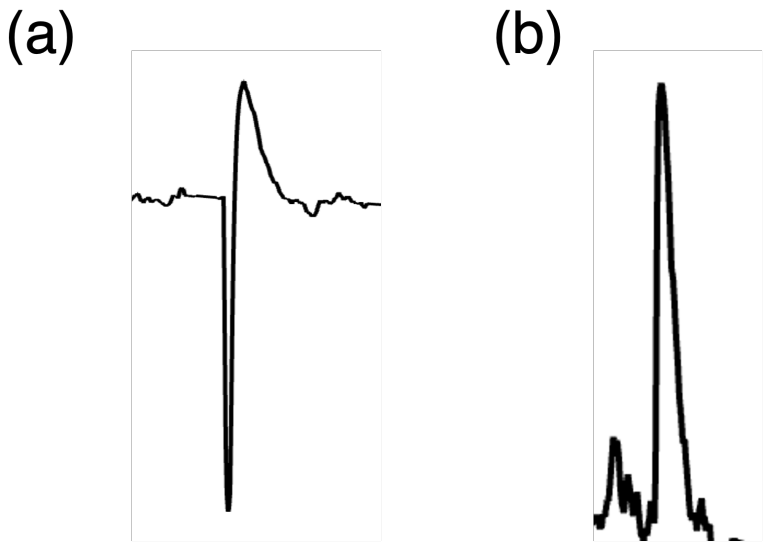

Figure 6.4: Typical astrocyte signals chosen to analyse. (a) Biphasic signal.(b) Monophasic signal.

In this study, the area of the signals is calculated using a tool available on the rcSoftware. One of the tool measurements is the total signal area (ΔA). This calculation is determined by the triangular or rectangular regions formed between the two consecutive data points that represent the beginning and end of the signal, which assumes that the baseline lies on the ordinate ($y = 0$). There are three possible cases:

- case 1, when both points are above the baseline ($y \geq 0$),
- case 2, when both points are below the baseline($y \leq 0$),
- case 3, when one point is above and the other below($y_0 \leq 0$ and $y_1 \leq 0$).

For case 1 and 2, when $y_0 = 0$ or $y_1 = 0$, the ΔA is given by,

$$\Delta A = \frac{\Delta P_{\{x_0,x_1\}} \times \Delta P_{\{y_0,y_1\}}}{2} \tag{6.1}$$

where ΔA is a triangular surface. If $y_0 \neq 0$ and $y_1 \neq 0$, the ΔA is given by the formula:

$$\Delta A = \Delta P_{\{x_0,x_1\}} \left(\min\{y_0, y_1\} + \frac{\max\{y_0, y_1\} - \min\{y_0, y_1\}}{2} \right) \tag{6.2}$$

where ΔA is the sum of a rectangular and a triangular surface, $\min\{y_0, y_1\}$ is the height of the rectangle is the lowest ordinate, and the difference between $\max\{y_0, y_1\}$ and $\min\{y_0, y_1\}$ is the height of the triangle.

Finally, in case 3, ΔA is the sum of two triangular regions, requiring the computation of the point of intersection with the baseline [85].

This tool facilitates the analysis of the area below the signal by calculating it automatically.

6.3 Results

6.3.1 Electrophysiological signal time series

Records of extended length were obtained over a span of several days. A typical electrophysiological signal time series obtained using the electrodes is shown in Figure 6.5. The activity is characterised by periods of intense activity that are often composed of discrete signals interspersed by periods of silence intervals. This kind of extended recording enabled the examination of the area of several signals indicated in Section 6.2.2 in order to assess the intercellular communication activity among astrocytes. To enhance this study, several recordings were conducted because a larger quantity of recorded signals indicates better communication since each signal corresponds to an ionic fluctuation linked to the activation of ion channels in the astrocytes.

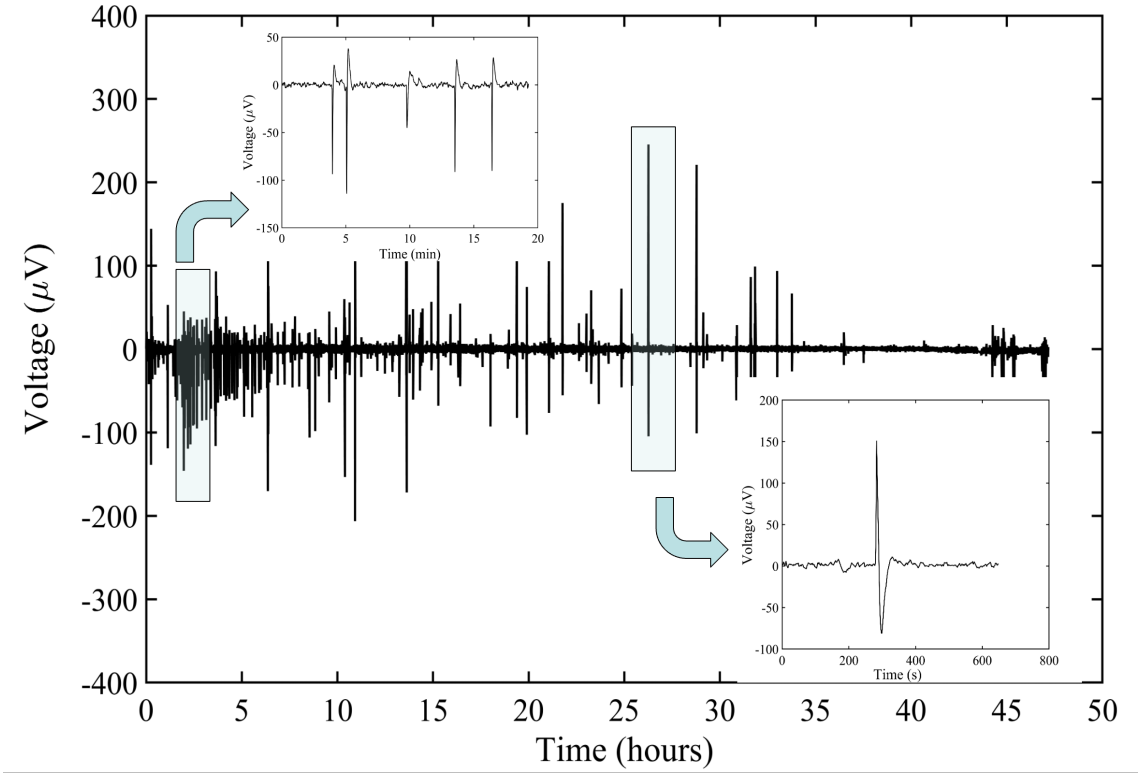

Figure 6.5: Typical record of bioelectrical activity measurements over several days.

Subsequently, the acquired findings of the research conducted to ascertain the potential correlation between the signal area and the shape and area of the electrode will be examined. This analysis will provide a better understanding of the processes that influence these bioelectrical phenomena.

6.3.2 Evaluation of the signals' area

This study aims to determine whether the area and geometry of the electrode influence the signal's area. The calculation of signal area, as explained in Section 6.2.2, is directly proportional to signal power, indicating that discussions on signal area basically refer to signal power from now on in this chapter. In order to achieve this, two distinct experiments with varying sensor architectures were analysed. The first experiment investigates the surface area of the circular electrode shown in (a) Round electrodes (IBIDI), while the second experiment examines the circular electrode's width, as shown in (b) Circular electrodes. In both experiments, many discrete signals across the electrode geometries and areas described in Chapter 5 were identified.

(a) Round electrodes (IBIDI)

Figure 6.6 displays the results corresponding to the area of the signals in the experiment conducted using four round electrodes with distinct active electrode areas. The histograms group the signals into bins with an area of 100 $s.\mu V$, which provides a clear distribution of the signal areas and frequencies for each electrode area.

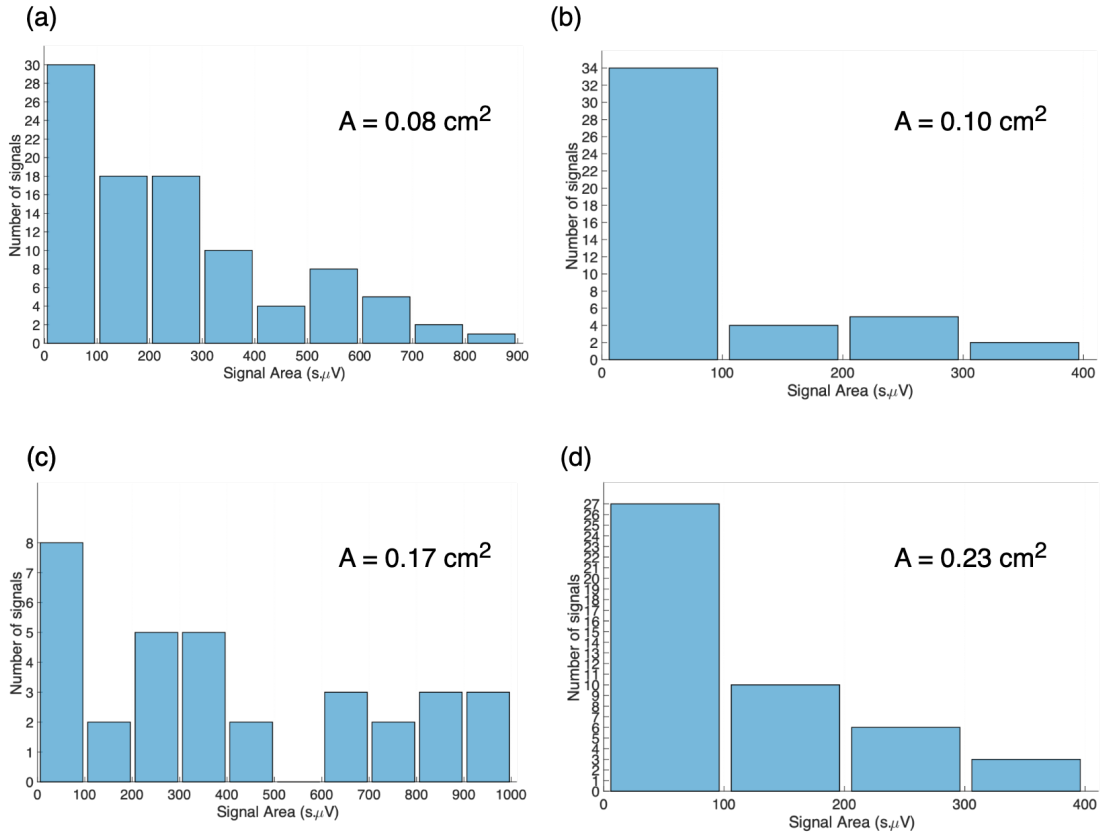

Figure 6.6: Comparison of the signal area for round electrodes with different electrode surface areas.The histograms show the distribution of signal areas ($s.\mu V$) for four electrode surface areas: (a) 0.08 cm^2, (b) 0.10 cm^2, (c) 0.17 cm^2, and (d) 0.23 cm^2.

The signal area measured using the smallest round electrode (Figure 6.6(a)) exhibited a wide range of distribution of signal area, with most values concentrated below 300 $s.\mu V$. The round electrode with an area of $0.17cm^2$ (Figure 6.6(c)) captured a larger range of the signal area. On the other hand, with the increase of the electrode area to $0.23cm^2$ (Figure 6.6(d)), the distribution became narrower, with most signals having an area below 400 $s.\mu V$. It is important to mention that the distribution for the results of the signals captured by the electrode with an area of $0.10cm^2$ has a similarity to the one with an area of $0.23cm^2$, since both have signals below 400 $s.\mu V$.

(b) Circular electrodes

The histograms in Figure 6.7, which group the signal area values into bins of 100 $s.\mu V$, display the results obtained using circular electrodes of four predetermined widths, following the same method as the round electrodes.

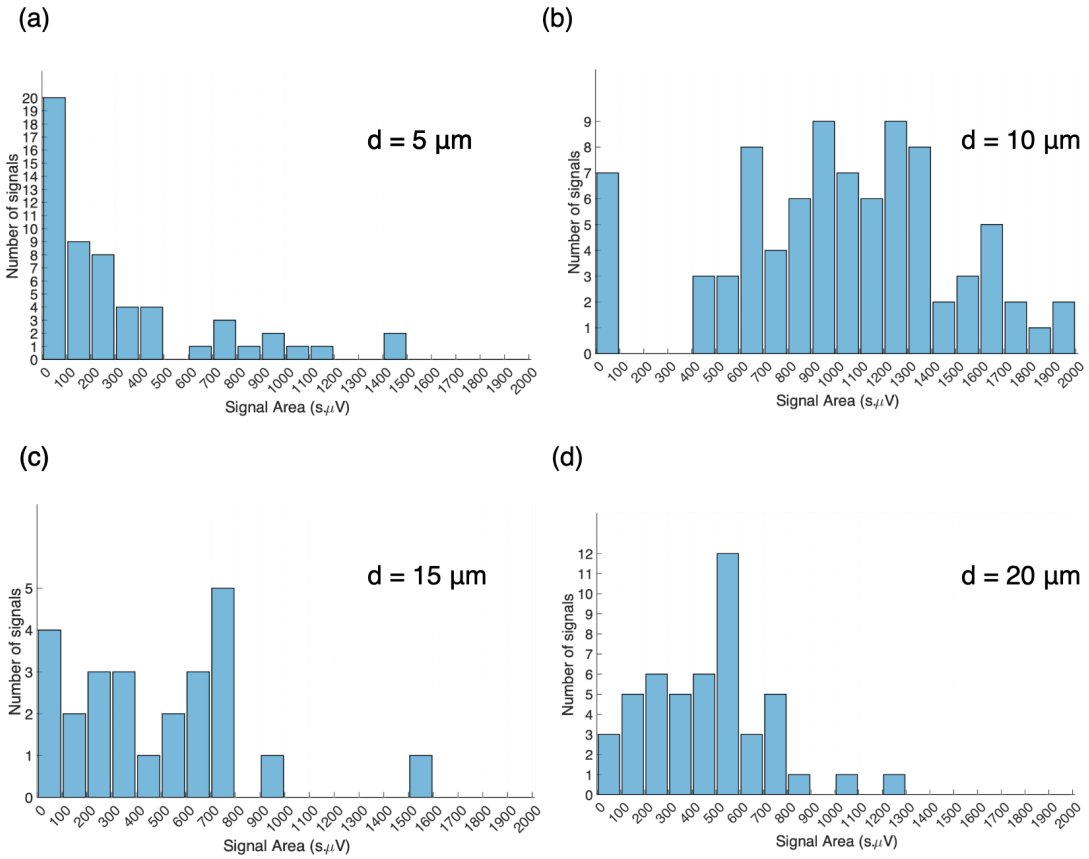

Figure 6.7: Comparison of the signal area for circular electrodes with different electrode widths.The histograms show the distribution of signal areas ($s.\mu V$) for four electrode widths: (a) 5 μm, (b) 10 μm, (c) 15 μm, and (d) 20 μm.

The electrode with the smallest width (Figure 6.7(a)) presents a distribution concentrated in smaller areas, with most signals having areas below 300 $s.\mu V$. With the increase of the electrode width to 10μm (Figure **??**(b)), the distribution expanded, showing a concentration between 600 and 1400 $s.\mu V$.

For the electrode with a width of 15μm (Figure 6.7(c)), the number of signals used to measure the area was lower. However, the signal area distribution presents more uniform form up to 400 $s.\mu V$. Finally, the electrode with the largest width (Figure 6.7(d)) showed a narrower distribution, with the majority of the signals with areas between 100 and 600 $s.\mu V$.

6.4 Discussion and Conclusions

This chapter gives an inside look at the experiments made to explore the impact of the electrode design on the duration of signals obtained from astrocyte cultures. The experiments focused on two different sensing structures: a commercial 8 Well PET array (IBIDI device) and circular electrodes. The first sensing electrode maintained a constant round geometry while systematically varying the active area. In contrast, the second design used a variety of circular electrodes with different widths. The hypothesis proposes that the electrode surface area and geometry can influence the signal area, with a focus on either cell synchronisation or the detection of travelling calcium waves.

The analyses of the discrete signals revealed a board range of signals, spanning from less than 10 $s.\mu m$ up to around 2000 $s.\mu m$. These signal areas were grouped into 100 $s.\mu m$ intervals, and the number of signals in each bin was evaluated. The results provided different insights for the two electrode designs. For the IBIDI electrodes, it was found that the power signal (signal area) did not exhibit a clear dependence on the electrode area since the signal distributions remained similar across the different areas. Observing the example of the electrodes with an area of $0.10cm^2$ and of $0.23cm^2$, it is visible the similar results in these two results.

In contrast, the results for the circular electrodes revealed that the power signal generally increased with lane width, indicating a possible relationship between electrode geometry and power signal. However, an exception was observed for the 15 μm width electrode, where the number of detected signals was lower and the distribution was more concentrated from up to 800 $s.\mu V$.

The methodology used to calculate signal areas used an established baseline, which was not always possible to obtain because some of the captured signals were not centred at y = 0. This could potentially impact the accuracy of the calculated areas. Future studies should consider updating the baseline definition or using more rigorous analytical tools to reduce this problem.

In conclusion, this study highlights the complexities of using extracellular electrodes to study intracellular communication in a population of astrocytes. It also reveals that while electrode geometry can influence the properties of these signals, this impact is not always clear. TThe round electrodes (IBIDI) did not show a clear relationship between signal area and geometry. This was probably due to astrocyte clustering and experimental noise. On the other hand, the circular electrodes suggested a partial correlation between lane width and power signal, with exceptions attributed to methodological limitations. The challenges in obtaining continuous populations of astrocytes through the electrodes make it difficult to detect travelling calcium waves and collective behaviour, highlighting the need to optimise electrode design, improve noise reduction, and enhance the methodology of area calculation. These results provide preliminary information, but they underline the need for further research to better understand the dynamics of the astrocytic network.

Chapter 7

Analysis of the Electrical Noise in Astrocyte Population

This chapter offers an analysis of electrical noise in a population of astrocytes. The study focuses on long-term recordings, characterised by bursts of activity intercalated by relatively silent regions. The different noisy regions are studied both in the time and frequency domains. In addition, it is observed that bursts of activity are initiated and terminated by master signals. This triggering and termination of the cell activity is discussed in the context of coordination signals.

7.1 Introduction

When a population of hundreds or even thousands of cells is connected in continuous layers measured, it is expected that not all the cells synchronise but instead remain uncoordinated. Therefore, discrete signals are not really expected. The average activity may resemble noise. It is possible that this electrical noise has different spectral properties that will allow us to distinguish between this biological noise and the intrinsic thermal noise generated by the sensing device, such as thermal and 1/f types of noise.

Biological noise in cell populations has been observed by several authors[101, 102, 103, 104, 105, 106, 107, 108, 109].Most writers describe this noise as fluctuations in the membrane potential of individual cells, which are not consistently stable in live cells due to minor oscillations caused by their continuous activity.

In the references provided, some authors ([103, 106, 107]) employed computational models and simulation models to analyse the bioelectrical noise in neuronal-astrocytic networks. Particularly in [103] was explored the influence of astrocytes in stochastic resonance (SR), which is the increased detection of weak signals in the presence of noise. It has been shown that astrocytes have the ability to regulate double SR, which represents the second highest peak in the neuronal detection of weak signals. This study results give information regarding the possible involvement of astrocytes in intrinsically noisy neuronal information processing. On the other hand, in [106], it was determined that astrocytes may modulate neuronal activity, which increases the performance of firing rate propagation in

environments that are noisy and weak. According to this study [106], the astrocytes may be seen as internal noise sources that work with weak signals from the outside to stop neurones in the same layer from firing at the same time and improve communication. In [107], the authors developed a cell-electrode interface noise model for high density MicroElectrode Arrays (MEAs) to improve the co-simulation of the cell-electrode electrical characteristics. They concluded that using materials such as Pt (platinum) and TiN (titanium nitrite) decreases the electrode noise at low frequencies.

The primary objective of this dissertation is to quantify bioelectrical activity utilising extracellular electrodes. Therefore, the analysis conducted in [104, 105, 108] seems more relevant to the bioelectrical noise under investigation. The authors in [104] show that it is feasible to identify cancerous from non-cancerous cells by evaluating the noise in real and imaginary electrical impedance, i.e., based on the properties of the electrical noise. They use small gold electrodes to capture the examined signals. In [108], snail neurones were cultured on chips coated with polylysine to show that thermal noise measurements could go beyond the effect of the sheet resistance. These measurements contributed to the observed changes in membrane conductance and capacitance. In the study [109], thermal noise at the cell-chip junction was also studied, but this time field-effect transistors were used. The authors interpreted the noise as Nyquist noise, a specific type of thermal noise. They concluded that this thermal noise from cell adhesion can help to better understand the electrical characteristics of the interface between nerve cells and transistors. Additionally, it establishes a thermodynamic threshold for the Signal-to-Noise Ratio (SNR) of neuroelectronic interfacing.

In contrast, in [105], the authors used needles to examine the signals. The researchers believed that the skin and muscle tissue with the electrodes generate random thermal noise that accurately reflects the fluctuations that occur when the subject is resting on a bed. In the end, it was determined that the equivalent impedance observed at certain frequencies corresponds to the thermal noise produced by the "polarisation cell" at those equivalent frequencies.

In this chapter, an explanation of the electrode used in this experiment will be provided, followed by an examination of a long-term recording of bioelectrical activity, with the major emphasis being the electrical noise.

7.2 Experimental

Astrocyte populations were used on the electrode arrays used to measure a week before. Astrocytes are sow-growing and take very long to form a confluent monolayer. Cells were only measured when a confluent monolayer was reached.

7.2.1 Graphene oxide electrode

Figure 7.1 shows the electrode design used in this study. In Figure 7.1(b) is a photograph of the entire electrode array fabricated in a glass substrate, and in Figure 7.1(b) is a photograph of the entire electrode array fabricated in a Silicon

Dioxide (SiO_2) substrate. As mentioned in chapter **??**, each substrate has five independent gold electrodes with a circular pattern. The gold electrodes were produced by thermal evaporation and lithography on top of the glass substrates. The middle electrode was used as a sensing electrode. This electrode has a round shape with a diameter of 60 micrometres (μm). This electrode is coated with a layer of Graphene Oxide (GO).

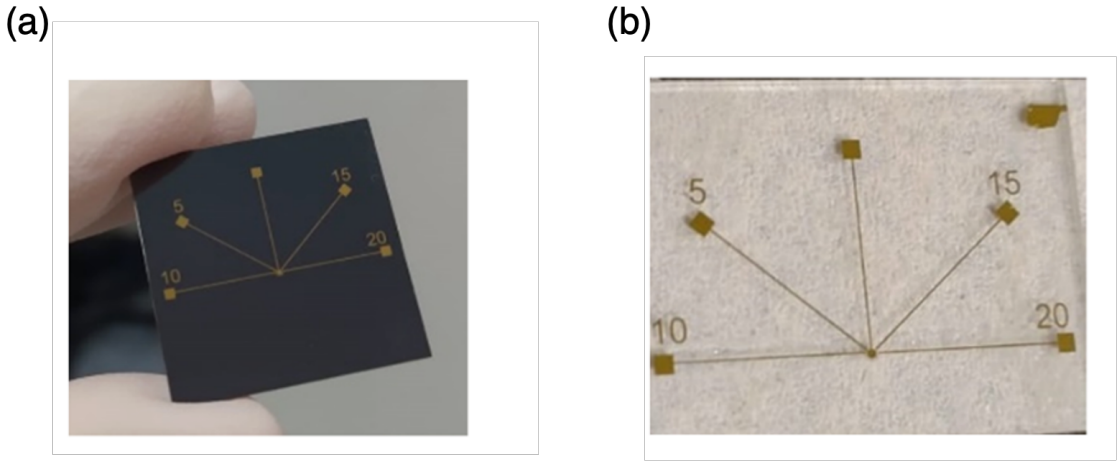

Figure 7.1: Entire electrode array. (a) Electrodes based on SiO_2. (b) Electrodes fabricated in a glass substrate.

The GO electrode used can be seen in Figure 7.2, and it was fabricated using the method of [110]. This method uses the GO solution that was made using a modified Hummer method. After that, GO solutions in water at concentrations of 1 or 2 mg ml^{-1} were spun at 2,000 r.p.m. over gold on glass (Kintec). These samples were previously cleaned using sonication at 60 °C in acetone and subsequently in isopropyl alcohol. They also were subjected to a clean treatment with air plasma.

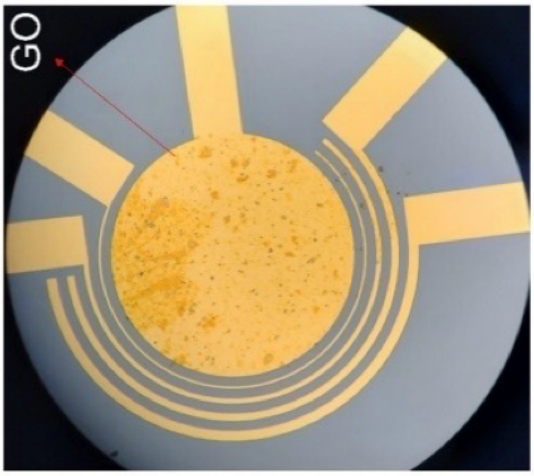

Figure 7.2: GO electrode

It is important to note that the authors in [110] believe that the GO electrode promotes the growth of astrocytes without any treatment.

To record the bioelectrical activity, the instrumentation described in Chapter **??** was used. Details of the device sample holder used in this experiment can be found in Section 4.1.1.

7.3 Results

7.3.1 General overview of long-term recordings

Here, we present and discuss several long-term recordings of astrocyte populations. In Figure 7.3, the recording shows the bioelectrical activity in an astrocyte population measured over 6 consecutive days. The overall time trace is characterised by intense bursts of activity separated by relatively quiet periods.

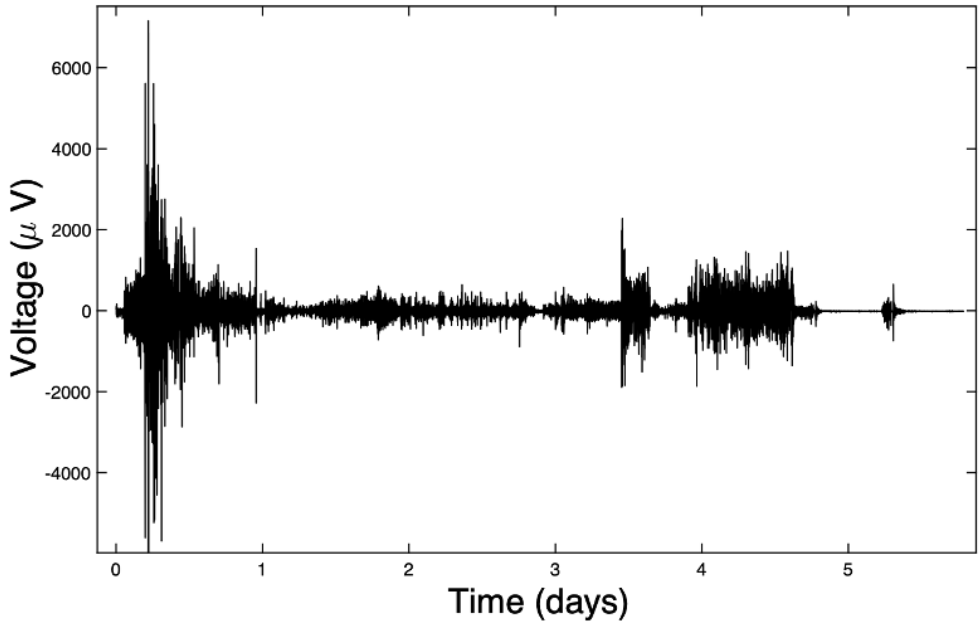

Figure 7.3: Overview of the recording of the bioelectrical activity in an astrocyte population

The measures of signal amplitude quantify the bioelectrical activity. This signal's quantification is expressed in microvolts (μV), ranging from around -5000 μV to 6000 μV.

Within the initial day, the astrocyte displayed increased levels of activity.This phenomenon may be attributed to the phase of their adaptation to the environment in which they were placed.

These signals are quantified and expressed in μV, ranging from around -5000 μV to 6000 μV.

During days 3 and 4, there is a surge in activity followed by a subsequent dip in signal amplitudes, suggesting a potential cessation of communication between the cells.

7.3.2 Detailed view of long-term recordings

In order to enhance the details of the analysis of this recording, it will be examined from two perspectives: silence regions and bursts of activity. Silence regions refer to specific time intervals during which astrocytes remain silent in extracellular communication. Bursts of activity are short periods of time characterised by a sudden increase in noise levels.

The long-term recording was analysed with the purpose of giving a clear perspective of the cell activity variation. The alteration is defined by a transition from solenced regions to bursts of activity or the reverse. In this research, the selected set clearly demonstrates the shift in activity, providing a clear perspective

for the reader.

Figure 7.4 shows the chosen set, which displays a silent region followed by a burst of activity. Observing Figure 7.4(a), it can be seen that there is a clear distinction between region A, representing the silence region, and region B, representing the burst of activity, i.e., the change in cell activity.

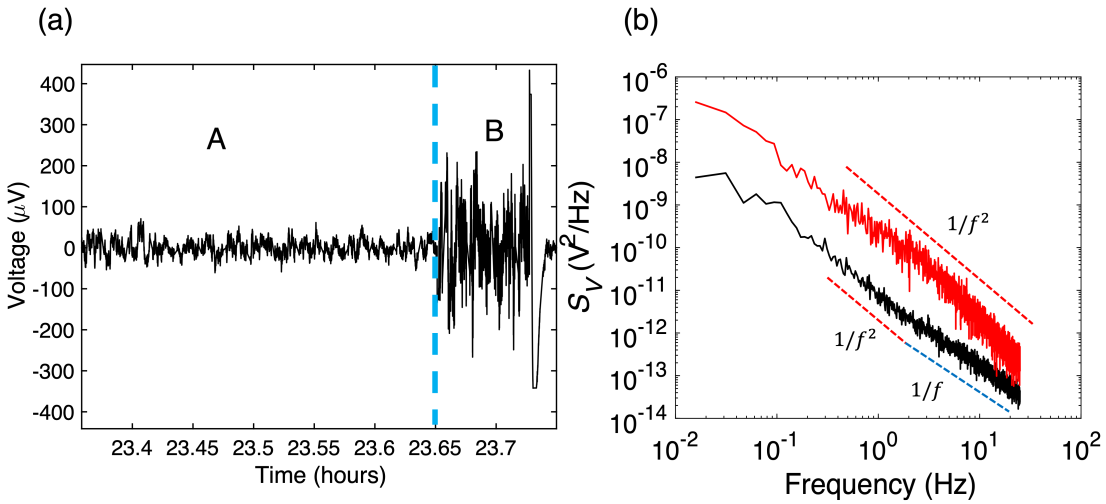

Figure 7.4: Set of a silent region, A, followed by a burst of activity, B. (a) Set in the time domain. (b)Power Spectral Density (PSD) of the silent region in black and PSD of the burst of activity in red.

In the case of frequency domain analysis, it can be concluded that the noise from region A to region B, at the higher frequencies, increases from $1/f$ to $1/f^2$. This conclusion can be reached from the analysis in Figure 7.4(b), which also shows that at lower frequencies the noise remains at $1/f^2$.

7.3.3 Trigger signals (Start and Stop Trigger Signals)

Upon analysing this experiment, it was observed that there were distinct signals that initiated and concluded the bursts. These signals enabled the easier detection of bursts and provided a clearer perspective on the duration of the bursts.

Observing Figure 7.5, it is possible to visualise this phenomenon, which contributes to the hypotheses that these signals coordinate the activity of the astrocytes' population study.

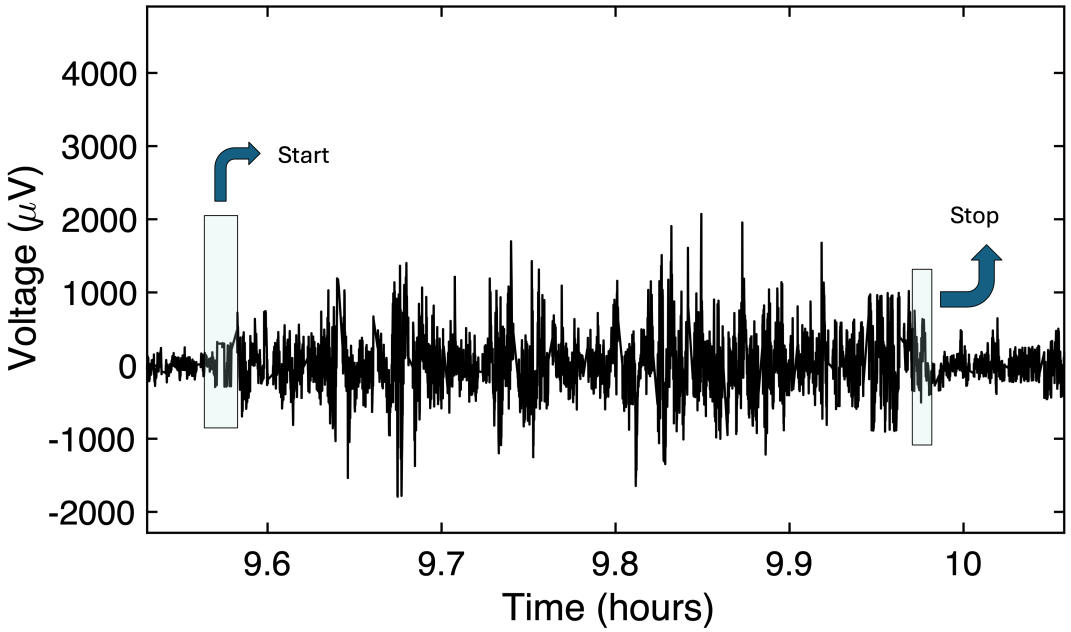

Figure 7.5: Burst of activity with the start trigger signal and its stop highlighted.

In order to confirm that after the occurrence of the trigger signals, the activity of the cells changes, several bursts were analysed. From this analysis, two signals were chosen, one that starts the burst and the other that ends the burst, with the objective of demonstrating this intensity change. Figure 7.6 shows a clear visualisation of the change in activity after the trigger signal that starts the burst. This signal, either because of the extracellular measurement system or because of biological noise, has been cut. For this reason, the start trigger signal reconstruction was inserted into Figure 7.6.

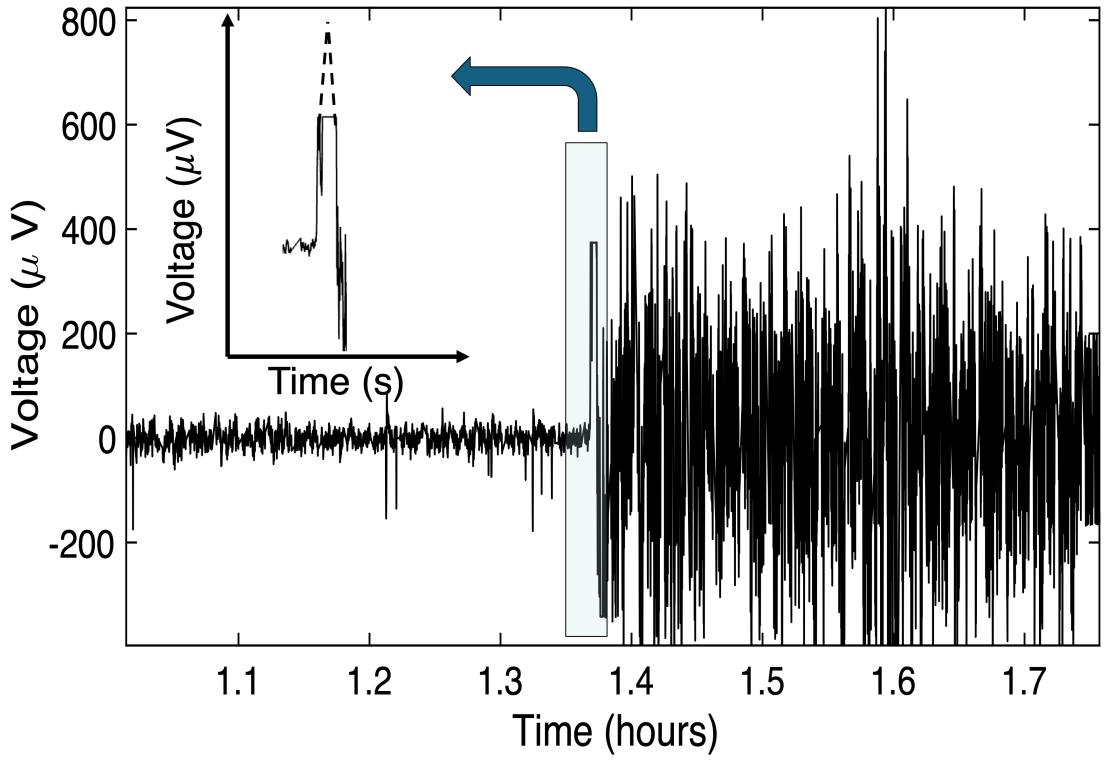

Figure 7.6: Overview of the start trigger signal of a burst of activity, with an inset plot highlighting the reconstruction of the signal.

The initial trigger signal is detected as a peak that was attenuated by the spectrum analyser at the very beginning of the burst, as indicated by the blue box in Figure 7.6. The inset plot offers an elaborate representation of this signal, revealing a sudden increase in voltage followed by a rapid restoration to the original level. The signal has a duration of approximately 18.72 seconds (s), and after reconstruction, the amplitude peaks are around 400 μV.

Figure 7.7 shows the trigger signal that stops the burst, which permits the visualisation of the decrease in cell activity after the signal occurred. For the same reason for the reconstruction of the trigger signal that starts the burst, the insert blue box highlights the reconstruction of the trigger signal that stops the burst.

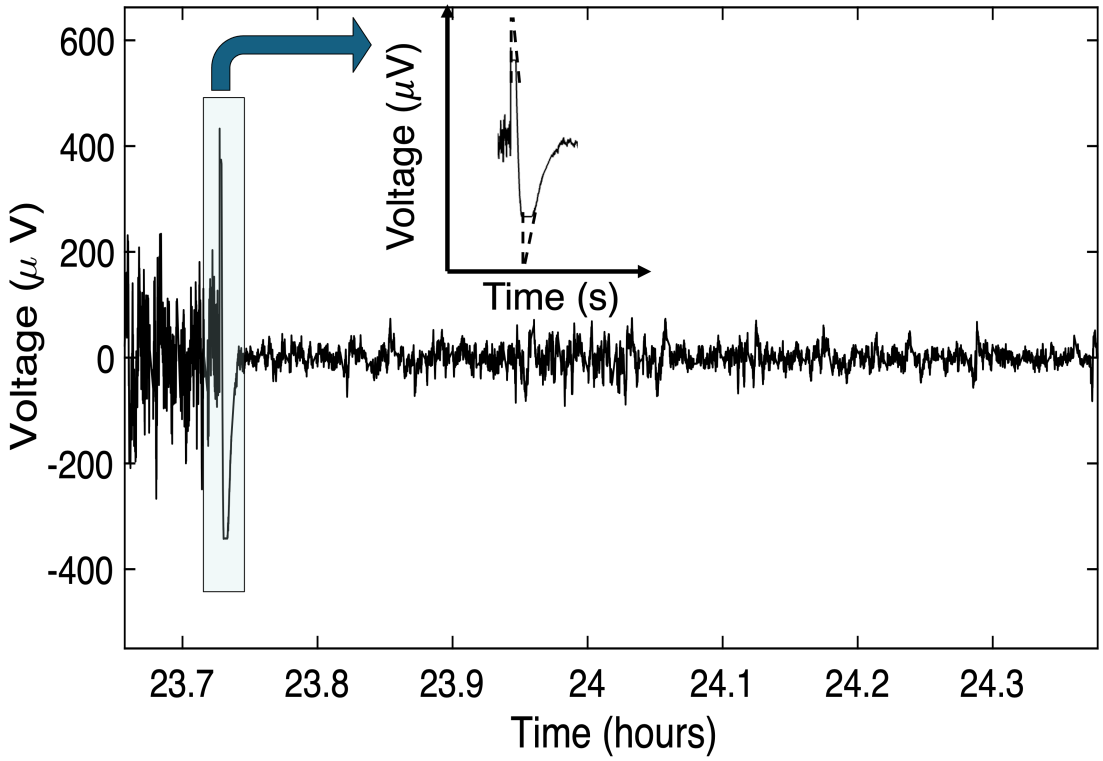

Figure 7.7: Overview of the stop trigger signal of a burst of activity, with an inset plot highlighting the reconstruction of the signal.

The additional plot, shown in figure 7.7, offers an improved visual representation of the stop trigger signal. This signal has a short duration of only 7.56 s. The peaks of amplitude reach around $500\mu V$.

7.4 Discussion

Long-term recordings of astrocyte populations are made using an electrode made of GO. The analysis of the long-term recording reveals periods of bioelectrical activity and periods of complete silence in intracellular communications. These variations of behaviour suggest that astrocyte populations go through different faces of pause and activation. As previously stated, it is believed that the initial high activation observed was due to the adaptation response of the astrocytes to the new environment and to the electrode adherence.

The examination of the astrocyte population's long-term recordings revealed that the majority of these signals were either noise or signals that the spectrum analyser suppressed, leading to the assumption that biological noise took place. To better understand the presented noise, the signals were divided into regions of when cells are in silence and when there are bursts of activity.

By focusing on the set of the combination of these two regions chosen, it becomes evident that at lower frequencies, both regions exhibit $1/f^2$ noise. At fre-

quencies above 1 Hertz (Hz), region A exhibits $1/f$ noise, while region B maintains $1/f^2$ noise.

An analysis of this astrocyte population's long-term recordings revealed the presence of trigger signals linked to the start and stop of bursts of activity, which remain incompletely understood. The spectrum analyser's range filtered out the majority of these signals. Through their reconstruction, it became possible to acquire the duration and amplitudes of the signals, which exhibited variations from one signal to another, lacking a consistent characteristic that would enable the identification of whether they were start or stop signals. Only by the activity preceding and following their occurrence could they be differentiated. Comparing the chosen trigger signal to analyse, the start signal had a longer duration than the stop signal. In terms of amplitude, both signals have around 400, 500 μV.

7.5 Conclusion

In sum, this chapter presented a concise review of the literature on biological noise, which facilitated a deeper comprehension of the origins of this noise. A brief description of the electrode and the measuring technique used in this experiment were included in the following sections.

An investigation of extended recordings from a population of astrocytes showed the bioelectrical signals specific to this cell type. The differentiation established between periods of silence and bursts of activity indicates that these cells do not exhibit a consistent pattern of bioelectrical activity. Conversely, they progress through phases of sleepiness and activity, thus reinforcing the idea that astrocytes play a crucial role in the brain.

Additionally, an analysis of the noise in a set of silence regions followed by a burst of activity was presented. It was found that the noise in these two areas is only different at frequencies above 1 Hz.

The detection of trigger signals at the beginning and end of the bursts of activity provided further intricacy to the comprehension of this astrocyte population. Although not fully comprehended, these signals indicate that they can tell us when the burst begins and when it ends.

Chapter 8

Conclusions and future work

This chapter focuses on the outlines and discusses the major findings of this thesis. It also presents some of the questions raised during this research, together with suggestions for experiments to elucidate them. Finally, it discusses how the methodology developed in this project can be applied in various areas.

8.1 Primary topics studied

This dissertation studies the bioelectrical signals recorded from astrocyte populations. This bioelectrical activity was recorded using extracellular electrodes and electrical low-noise recording techniques, with the aim of obtaining knowledge about the nature of the electrical oscillations generated by interconnected astrocytes.

This study involved three key experiments. In the first study, the evaluation of the signal format was observed, and the power of a typical biphasic signal in the captured extracellular signals was determined.The second experiment aimed to answer a key question: Does the design and geometry of electrodes influence the characteristics of the recorded signals, particularly their power? The third experiment examined the electrical noise present in the extracellular recordings of a population of astrocytes.

The next section provides a concise description of these experiments and their principal results.

8.2 Conclusions

The studies were divided into three components to improve the explanation of their conclusions: (a) investigation of signals and their power order magnitude; (b) the influence of the electrode on the distribution of bioelectric signals; and (c) examination of electrical noise within the astrocyte population.

(a) Investigation of signals and their power order magnitude

A characterisation of the signal types detected in the measurements was conducted, revealing a possible evolution of monophasic signals to biphasic, although this remains unproven.

In this analysis, a signal equivalent in length and amplitude to the usual biphasic signals seen in this research was created. This signal was created to determine the order of magnitude of the power of a biphasic signal. The signal's power was computed using two methods, both yielding identical results. The results show that the order of magnitude of the signal's power is nano (10^{-9}).

(b) The influence of the electrode on the distribution of bioelectric signals

The experimental study on electrode design's impact on bioelectric signal detection highlighted the complex relationship between electrode geometry, surface area, and signal power distribution (area under the signal). The main results showed that the design of the electrodes might change the strength and spread of bioelectric signals, but this connection was complicated and depended on things like cell adhesion and experimental noise.

For round electrodes (IBIDI), the power signal distribution remained largely unaffected by variations in electrode surface area, with similar results observed for electrodes of $0.10cm$ and $0.23cm$. The natural clustering of astrocytes tended to aggregate in specific areas rather than uniformly spreading across the electrode surface. This hides the potential effects of the electrode's size and contributes to this lack of variation.

In contrast, circular electrodes demonstrate a consistent pattern of increasing power signals with the lane width, suggesting that the electrode geometry influences the capture of larger or more numerous synchronised cell clusters. Nonetheless, the electrode with $15\mu m$ width differs from this pattern, exhibiting a reduced number of detected signals and a more concentrated distribution.

It is important to mention that a non-confluent cell monolayer cannot support travelling waves. Several experiments in this study failed to reach the confluent monolayer, potentially leading to the inconclusive findings.

(c) Examination of electrical noise within the astrocyte population

This research examined the bioelectrical activity of astrocyte populations, emphasising the examination of electrical noise over extended recordings. This research investigates the characteristics of noise in two separate contexts: periods of silence and bursts of activity. At frequencies below 1 Hz, the observed noise is characterised as $1/f^2$ noise in both regions. Nevertheless, when the frequency increased, the characteristics of the noise varied. In the silent region, the noise changes to $1/f$, but during the bursts of activity, it persists at $1/f^2$.

The investigation also identified master signals, or trigger signals, that marked transitions between periods of silence and bursts of activity. These signals provided important information about the beginning and end of bursts and acted as indicators of the behavioural changes in the astrocyte population. The interruption of these signals could potentially be due to the recording system or biological noise. It's important to note that the origins of these signals remain unclear.

8.3 Future Investigations

The results and their evaluations suggest that more research is required to further this study.The following subparagraphs define the suggested steps for approaching future tasks.

(a) Further evaluation on the shape of the bioelectrical signals

This study investigated the possible evolution of signals from monophasic to biphasic. To enhance comprehension of this discovery and verify its accuracy, a more thorough examination is necessary to clarify the origins of biphasic signals. For example, instead of relying solely on one type of biphasic signal and another nomophasic signal for the power analysis to evaluate the working hypothesis, it would be beneficial to incorporate all the identified signal types.

(b) Data analysis of the signal properties

The distribution of signal parameters must continue to be conducted in terms of signal power. It is essential to update the methodology for calculating signal power, as the current baseline is inadequate due to the signal's observed base not being $y = 0$.Furthermore, all experiments must be conducted only after a complete confluent monolayer has been established.

(c) Bioelectrical activity of astrocyte-neuron co-cultures

This dissertation primarily sought to quantify the coculture of astrocytes and neurones. However, difficulties in producing confluent astrocyte monolayers prevented the inclusion of the co-culture evaluation in this thesis. Future studies should capture and analyse the bioelectrical signals of co-cultures to gain significant insights into the function of astrocytes within brain networks.

Bibliography

[1] Yilda Irizarry-Valle and Alice Cline Parker. An astrocyte neuromorphic circuit that influences neuronal phase synchrony. *IEEE Transactions on Biomedical Circuits and Systems*, 9(2):175–187, 2015.

[2] George Martin, Jim Harkin, Liam J. McDaid, John J. Wade, and Junxiu Liu. On-chip communication for neuro-glia networks. *IET Computers & Digital Techniques*, 12(5):255–263, 2018. Special Section: Bio-inspired Hardware and Evolvable Systems.

[3] Susanna Yu. Gordleeva, Yuliya A. Tsybina, Mikhail I. Krivonosov, Mikhail V. Ivanchenko, Alexey A. Zaikin, Victor B. Kazantsev, and Alexander N. Gorban. Modeling working memory in a spiking neuron network accompanied by astrocytes. *Frontiers in Cellular Neuroscience*, 15:631485, 2021.

[4] C Fewtrell. Ca2+ oscillations in non-excitable cells. *Annual Review of Physiology*, 55(1):427–454, 1993. PMID: 8385436.

[5] Nataly Hastings, Yi Lin Yu, Botian Huang, Sagnik Middya, Misaki Inaoka, Nadia A. Erkamp, Roger J. Mason, Alejandro Carnicer-Lombarte, Saifur Rahman, Tuomas P.J. Knowles, Manohar Bance, George G. Malliaras, and Mark R.N. Kotter. Electrophysiological in vitro study of long-range signal transmission by astrocytic networks. *Advanced Science*, 10, 10 2023.

[6] Ana L.G. Mestre, Pedro M.C. Inácio, Youssef Elamine, Sanaz Asgarifar, Ana S. Lourenço, Maria L.S. Cristiano, Paulo Aguiar, Maria C.R. Medeiros, Inês M. Araújo, João Ventura, and Henrique L. Gomes. Extracellular electrophysiological measurements of cooperative signals in astrocytes populations. *Frontiers in Neural Circuits*, 11, 10 2017.

[7] An electrical method to measure low-frequency collective and synchronized cell activity using extracellular electrodes. *Sensing and Bio-Sensing Research*, 10:1–8, 9 2016.

[8] Younghee Kim, Jang-Soo Park, and Yun Kyu Choi. The role of astrocytes in the central nervous system focused on bk channel and heme oxygenase metabolites: A review. *Antioxidants (Basel)*, 8(5):121, 2019. Published 2019 May 5.

[9] Junliang Jiang, Miaoxian Yang, Mi Tian, Zhong Chen, Lei Xiao, and Ye Gong. Intertwined associations between oxytocin, immune system and major depressive disorder. *Biomedicine & Pharmacotherapy*, 163:114852, 2023.

[10] Rosalia Siracusa, Rosanna Fusco, and Salvatore Cuzzocrea. Astrocytes: Role and functions in brain pathologies. *Frontiers in Pharmacology*, 10:1114, 2019. Published 27 September 2019.

[11] Erwin Neher and Bert Sakmann. Single-channel currents recorded from membrane of denervated frog muscle fibres. *Nature*, 260:799–802, 1976.

[12] Fredrick J. Sigworth. Single na+ channel currents. *Nature*, 287:447–449, 1980.

[13] Katherine L. Perkins. Cell-attached voltage-clamp and current-clamp recording and stimulation techniques in brain slices. volume 154, pages 1–18, 6 2006.

[14] E. Neher B. Sakmann O. P. Hamill, A. Marty and F. J. Sigworth. Improved patch-clamp techniques for high-resolution current recording from cells and cell-free membrane patches. volume 391, pages 85–100, 1981.

[15] Sanaz Asgarifar. *Ultra-sensitive Bioelectronic Transducers for Extracellular Electrophysiological Studies*. PhD thesis, University of Algarve, Faro, Portugal, 2018. Doctor of Philosophy in Electronics and Telecommunications.

[16] F.N. Quandt and B.A. MacVicar. Calcium activated potassium channels in cultured astrocytes. *Neuroscience*, 19(1):29–41, 1986.

[17] Joachim Bormann and Helmut Kettenmann. Patch-clamp study of γ-aminobutyric acid receptor cl^- channels in cultured astrocytes. *Proceedings of the National Academy of Sciences of the United States of America*, 85(23):9336–9340, 1988.

[18] Hao Yang Song Cao Yiting Luo Tian Yu Jie Yuan, You Zhang. Astrocytes are involved in the effects of ketamine on synaptic transmission in rat primary somatosensory cortex. *JIN*, 22(5):116–null, 2023.

[19] Makoto Taketani and Michel Baudry, editors. *Advances in Network Electrophysiology: Using Multi-Electrode Arrays*. Springer, Berlin, Heidelberg, 2006.

[20] A. aszcz, W. Nogala, A. Czerwiski, J. Ratajczak, and J. Ktcki. Fabrication of electrochemical nanoelectrode for sensor application using focused ion beam technology. *Polish Journal of Chemical Technology*, 16(3):40–44, 2014.

[21] W.-C. Li, S. R. Soffe, and Alan Roberts. A direct comparison of whole cell patch and sharp electrodes by simultaneous recording from single spinal neurons in frog tadpoles. *Journal of Neurophysiology*, 92(1):380–386, 2004.

[22] Marie Engelene J. Obien, Kosmas Deligkaris, Torsten Bullmann, Douglas J. Bakkum, and Urs Frey. Revealing neuronal function through microelectrode array recordings. volume 9, page 423. Frontiers Media S.A., 2015.

[23] Douglas J. Bakkum, Urs Frey, Milos Radivojevic, Thomas L. Russell, Jan Müller, Michele Fiscella, Hirokazu Takahashi, and Andreas Hierlemann. Tracking axonal action potential propagation on a high-density microelectrode array across hundreds of sites. *Nature Communications*, 4, 2013.

[24] High-resolution cmos mea platform to study neurons at subcellular, cellular, and network levels. *Lab on a Chip*, 15:2767–2780, 7 2015.

[25] Vishalini Emmenegger, Marie Engelene J. Obien, Felix Franke, and Andreas Hierlemann. Technologies to study action potential propagation with a focus on hd-meas. *Frontiers in Cellular Neuroscience*, 13, 4 2019.

[26] Takashi Kuroda, Nobuyuki Matsuda, Yu Ishibashi, and Ikuro Suzuki. Detection of astrocytic slow oscillatory activity and response to seizurogenic compounds using planar microelectrode array. *Frontiers in Neuroscience*, 16:1050150, 2023. Published 10 January 2023.

[27] Yang You, Kathleen Borgmann, Venkata Viswanadh Edara, Satomi Stacy, Anuja Ghorpade, and Tsuneya Ikezu. Activated human astrocyte-derived extracellular vesicles modulate neuronal uptake, differentiation and firing. *Journal of Extracellular Vesicles*, 9(1):1706801, 2020.

[28] Jonathan V. Choi, Biana K. Tchernookova, Vivek Kumar, Leon Kiedrowski, Cassie Goeke, Marina Guizzetti, Jennifer Larson, Michelle A. Kreitzer, and Robert Paul Malchow. Extracellular atp-induced alterations in extracellular h^+ fluxes from cultured cortical and hippocampal astrocytes. *Frontiers in Cellular Neuroscience*, 15:640217, 2021. Published 30 April 2021.

[29] Patrick A. Cody, James R. Eles, Carl F. Lagenaur, Takashi D.Y. Kozai, and X. Tracy Cui. Unique electrophysiological and impedance signatures between encapsulation types: An analysis of biological utah array failure and benefit of a biomimetic coating in a rat model. *Biomaterials*, 161:117–128, 2018.

[30] Richard A. Normann and Eduardo Fernandez. Clinical applications of penetrating neural interfaces and utah electrode array technologies. *Journal of Neural Engineering*, 13(6):061003, 2016.

[31] Morgan Ferguson, Dhavan Sharma, David Ross, and Feng Zhao. A critical review of microelectrode arrays and strategies for improving neural interfaces. *Advanced Healthcare Materials*, 8(19):1900558, 2019.

[32] David Kleinfeld, Milos Radivojevic, Felix Franke, Michael Altermatt, Jan Mü, Andreas Hierlemann, and Douglas J Bakkum. Tracking individual action potentials throughout mammalian axonal arbors. 2013.

[33] Jelena Dragas, Vijay Viswam, Amir Shadmani, Yihui Chen, Raziyeh Bounik, Alexander Stettler, Milos Radivojevic, Sydney Geissler, Marie Engelene J. Obien, Jan Müller, and Andreas Hierlemann. In vitro multifunctional microelectrode array featuring 59 760 electrodes, 2048 electrophysiology channels, stimulation, impedance measurement, and neurotransmitter detection channels. *IEEE Journal of Solid-State Circuits*, 52:1576–1590, 6 2017.

[34] Jiaru Fang, Shuang Huang, Fanmao Liu, Gen He, Xiangling Li, Xinshuo Huang, Hui jiuan Chen, and Xi Xie. Semi-implantable bioelectronics. *Nano-Micro Letters*, 14(1):125, 2022.

[35] Valentin A. Pavlov and Kevin J. Tracey. Bioelectronic medicine: updates, challenges and paths forward. *Bioelectronic Medicine*, 5(1):1, 2019.

[36] David M. Hillis, David Sadava, H. Craig Heller, and Sally D. Hacker. *Life: The Science of Biology*. Sinauer Associates, Sunderland, MA, 12th edition, 2019.

[37] Scott Freeman, Kim Quillin, Lizabeth Allison, Michael Black, Emily Taylor, Greg Podgorski, and Jeff Carmichael. *Biological Science*. Pearson, London, 6th edition, 2017.

[38] Nicole Gleichmann. Prokaryotes vs eukaryotes: What are the key differences?, June 2024. Accessed: 27-11-2024.

[39] Sheena E. B. Tyler. Natures electric potential: A systematic review of the role of bioelectricity in wound healing and regenerative processes in animals, humans, and plants. *Frontiers in Physiology*, 8:627, 2017.

[40] Nurdan Özkucur, Hans-Henning Epperlein, and Richard H. W. Funk. Ion imaging during axolotl tail regeneration in vivo. *Developmental Dynamics*, 239(7):2048–2057, Jul 2010.

[41] T. C. Südhof. Neurotransmitter release: The last millisecond in the life of a synaptic vesicle. *Neuron*, 80(3):675–690, 2013.

[42] A. Kimberley McAllister. Dynamic aspects of cns synapse formation. *Annual Review of Neuroscience*, 30:425–450, 2007.

[43] Duke University. Astrocytes orchestrate neural connections, Nov 2017. Accessed: 27-Nov-2024.

[44] Grégory Dallérac, Juan Zapata, and Nathalie Rouach. Versatile control of synaptic circuits by astrocytes: where, when and how? *Nature Reviews Neuroscience*, 19:729–743, 2018. Published: 06 November 2018.

[45] Louise Adermark and David M. Lovinger. Electrophysiological properties and gap junction coupling of striatal astrocytes. *Neurochemistry International*, 52(7):1365–1372, 2008.

[46] M.V.L. Bennett, L.C. Barrio, T.A. Bargiello, D.C. Spray, E. Hertzberg, and J.C. Sáez. Gap junctions: New tools, new answers, new questions. *Neuron*, 6(3):305–320, 1991.

[47] Heather D.E. Booth, Warren D. Hirst, and Richard Wade-Martins. The role of astrocyte dysfunction in parkinsons disease pathogenesis. *Trends in Neurosciences*, 40(6):358–370, 2017.

[48] W. W. Chen, X. Zhang, and W. J. Huang. Role of neuroinflammation in neurodegenerative diseases (review). *Molecular Medicine Reports*, 13(4):3391–3396, 2016.

[49] Peter M. Rappold and Kim Tieu. Astrocytes and therapeutics for parkinson's disease. *Neurotherapeutics: The Journal of the American Society for Experimental NeuroTherapeutics*, 7(4):413–423, 2010.

[50] Alexei Verkhratsky, Markel Olabarria, Harun N. Noristani, Chia-Yu Yeh, and Jose Julio Rodriguez. Astrocytes in alzheimer's disease. *Neurotherapeutics*, 7(4):399–412, 2010. Glial-Based Neurotherapeutics.

[51] Michael D. Monterey, Haichao Wei, Xizi Wu, and Jia Qian Wu. The many faces of astrocytes in alzheimer's disease. *Frontiers in Neurology*, 12, 2021. Published: 31 August 2021.

[52] A. M. Haidet-Phillips, M. E. Hester, C. J. Miranda, K. Meyer, L. Braun, A. Frakes, S. Song, S. Likhite, M. J. Murtha, K. D. Foust, M. Rao, A. Eagle, A. Kammesheidt, A. Christensen, J. R. Mendell, A. H. Burghes, and B. K. Kaspar. Astrocytes from familial and sporadic als patients are toxic to motor neurons. *Nature Biotechnology*, 29(9):824–828, 2011.

[53] M. Nagai, D. B. Re, T. Nagata, A. Chalazonitis, T. M. Jessell, H. Wichterle, and S. Przedborski. Astrocytes expressing als-linked mutated sod1 release factors selectively toxic to motor neurons. *Nature Neuroscience*, 10(5):615–622, 2007.

[54] Ralph van Passel, Wim AJM Schlooz, Karel JB Lamers, Wim AJG Lemmens, and Jan J Rotteveel. S100b protein, glia and gilles de la tourette syndrome. *European Journal of Paediatric Neurology*, 5(1):15–19, 2001.

[55] C. de Leeuw, A. Goudriaan, A. Smit, and et al. Involvement of astrocyte metabolic coupling in tourette syndrome pathogenesis. *European Journal of Human Genetics*, 23:1519–1522, 2015.

[56] Richard H. W. Funk. Endogenous electric fields as guiding cue for cell migration. *Frontiers in Physiology*, 6, 2015.

[57] Cinnamon L. VanPutte, Jennifer L. Regan, Andrew P. Russo, Rod Seeley, Trent Stephens, and Philip Tate. *Seeley's Anatomy and Physiology*. McGraw-Hill Education, 10th edition, 2014. Special Edition for North Carolina Central University.

[58] D. S. Adams and M. Levin. Endogenous voltage gradients as mediators of cell-cell communication: strategies for investigating bioelectrical signals during pattern formation. *Cell and Tissue Research*, 352(1):95–122, 2013.

[59] Christof Koch, Moshe Rapp, and Idan Segev. A brief history of time (constants). *Cerebral Cortex*, 6(2):93–101, 03 1996.

[60] Stony Brook University. Membrane potential – equivalent circuits, 2024. Acessado em: 28 de novembro de 2024.

[61] Xinzhu Yu, Jun Nagai, and Baljit S. Khakh. Improved tools to study astrocytes. *Nature Reviews Neuroscience*, 21(3):121–138, March 2020. Funding Information: The authors are supported by the US National Institutes of Health (NS111583, DA047444, NS060677 and MH104069), a Paul G. Allen Distinguished Investigator Award and the CHDI Foundation (to B.S.K.). B.S.K. was also partly supported by the Ressler Family Foundation. X.Y.

was supported partly by an American Heart Association Postdoctoral Fellowship (16POST27260256). J.N. was partly supported by a Japan Society for the Promotion of Science (JSPS) Overseas Research Fellowship (H28-729) and the Uehara Memorial Foundation Overseas Postdoctoral Research Fellowship (201730082). The authors regret that many papers could not be cited (especially early studies), because of space limits and the requirement to focus primarily on the past 5 years. The authors thank members of the Khakh laboratory for useful discussions, and the anonymous reviewers for their comments. Publisher Copyright: © 2020, Springer Nature Limited. Copyright: Copyright 2020 Elsevier B.V., All rights reserved.

[62] Ultrasensitive gold micro-structured electrodes enabling the detection of extra-cellular long-lasting potentials in astrocytes populations. volume 7. Nature Publishing Group, 12 2017.

[63] Mahmoud M.M. Ahmed and Toyoko Imae. Chapter 10 - graphene-based nanolayers toward energy storage device. In Toyoko Imae, editor, *Nanolayer Research*, pages 353–389. Elsevier, Amsterdam, 2017.

[64] I. Prigogine and Stuart A. Rice, editors. *Advances in Chemical Physics*. Advances in Chemical Physics. John Wiley & Sons, Inc., 1990.

[65] William M. Siu and Richard S. C. Cobbold. Basic properties of the electrolytesiosi system: Physical and theoretical aspects. *IEEE Transactions on Electron Devices*, 26(11):1805–1815, 1979.

[66] D.A. Stenger and T.M. McKenna. *Enabling Technologies for Cultured Neural Networks*. Number vol. 1 in Enabling Technologies for Cultured Neural Networks. Academic Press, 1994.

[67] J. E. B. Randles. Kinetics of rapid electrode reactions. *Discuss. Faraday Soc.*, 1:11–19, 1947.

[68] J.O.M. Bockris, A.K.N. Reddy, and M.E. Gamboa-Aldeco. *Modern Electrochemistry 2A: Fundamentals of Electrodics*. Modern electrochemistry. Springer US, 2001.

[69] C. D. Motchenbacher and J. A. Connelly. *Low-Noise Electronic System Design*. Wiley-Interscience, New York, 1993.

[70] J. B. Johnson. Thermal agitation of electricity in conductors. *Nature*, 119(2984):50–51, 1927.

[71] H. Nyquist. Thermal agitation of electric charge in conductors. *Phys. Rev.*, 32:110–113, Jul 1928.

[72] L. Moura, L.M. da Silva Carvalho de Moura, and I. Darwazeh. *Introduction to Linear Circuit Analysis and Modelling: From DC to RF*. Electronics & Electrical. Newnes, 2005.

[73] R. C. Gesteland, B. Howland, J. Y. Lettvin, and W. H. Pitts. Comments on microelectrodes. *Proceedings of the IRE*, 47(11):1856–1862, 1959.

[74] M.S. Keshner. 1/f noise. *Proceedings of the IEEE*, 70(3):212–218, 1982.

[75] Benjamin Lindner. Effects of noise in excitable systems. *Physics Reports*, 392:321–424, 03 2004.

[76] Edoardo Milotti. 1/f noise: a pedagogical review. *arXiv*, 2002.

[77] D. L. Gilden, T. Thornton, and M. W. Mallon. 1/f noise in human cognition. *Science*, 267(5205):1837–1839, 1995.

[78] A.A. Verveen and H.E. Derksen. Fluctuation phenomena in nerve membrane. *Proceedings of the IEEE*, 56(6):906–916, 1968.

[79] Alberto Carpinteri, Giuseppe Lacidogna, and Federico Accornero. Fluctuations of 1/f noise in damaging structures analyzed by acoustic emission. *Applied Sciences*, 8:1685, 09 2018.

[80] Tao Chen, Peter A. Bobbert, and Wilfred G. van der Wiel. 1/f noise and machine intelligence in a nonlinear dopant atom network. *Small Science*, 1(3), 2021.

[81] Tibor Grasser, editor. *Noise in Nanoscale Semiconductor Devices*. Springer Cham, Cham, Switzerland, 1 edition, 2020.

[82] F.N. Hooge. 1/f noise sources. *IEEE Transactions on Electron Devices*, 41(11):1926–1935, 1994.

[83] Stanford Research Systems. Sr560 - low-noise voltage preamplifier, 2024. Accessed: 11 October 2024.

[84] Keysight Technologies. 35670a fft dynamic signal analyzer, dc-102.4 khz (obsolete), 2024. Accessed: 11 October 2024.

[85] Pedro Miguel Cavaco Carrilho dos Santos Inácio. *Extracellular electrical transducers for recording signals of cells in culture*. phdthesis, Universidade do Algarve, Faro, Portugal, 2023.

[86] Fluke Corporation. *Programmable Automatic RCL Meter PM6306: Programmers Manual*, 960508 edition, 1996. Accessed: 15 October 2024.

[87] Fluke Corporation. *Programmable Automatic RCL Meter PM6306: Users Manual*, rev. 2, 02/99 edition, 1999. Accessed: 15 October 2024.

[88] American Type Culture Collection (ATCC). C8-d1a [astrocyte type i clone] (crl-2541). `https://www.atcc.org/products/crl-2541`, 2024. Accessed: 15 October 2024.

[89] Abhijit Patil, Rajesh Langoju, Suresh Joel, Bhushan D. Patil, and Sahika Genc. Biomedical signal analysis. In Chandan K. Reddy and Charu C. Aggarwal, editors, *Healthcare Data Analytics*, pages 127–177. Chapman & Hall, Boca Raton, FL, 2020.

[90] Radovan Martinek, Michaela Ladrova, Martina Sidikova, Robert Jaros, Kazem Behbehani, Radka Kahankova, and Agnieszka Kawala-Sterniuk. Advanced bioelectrical signal processing methods: Past, present and future approach-part i: Cardiac signals. *Sensors (Basel)*, 21(15):5186, 2021. Published 30 July 2021.

[91] Mariana de Sousa Fernandes. *Photonic Platform for Bioelectric Signal Acquisition on Wearable Devices*. Tese de doutorado, Universidade do Minho, Escola de Engenharia, Braga, Portugal, 2011. Orientadores: Paulo Mateus Mendes e José Higino Correia.

[92] John G. Proakis and Masoud Salehi. *Fundamentals of Communication Systems*. Pearson Education, Inc., Upper Saddle River, NJ, 2nd edition, 2014.

[93] Joel B. Harley. Eee 5502: Foundations of digital signal processing. `https://smartdata.ece.ufl.edu/eee5502/index.html`, 2022. Acessado em 19 de novembro de 2024.

[94] MathWorks. *trapz*, 2024. Disponível em: `https://mathworks.com/help/matlab/ref/trapz.html` [Acessado em 19 de novembro de 2024].

[95] Eliana Scemes and Christian Giaume. Astrocyte calcium waves: what they are and what they do. *Glia*, 54(7):716–725, 2006. Published 15 November 2006.

[96] Yossi Buskila, Andrea Bellot-Saez, and John W. Morley. Generating brain waves, the power of astrocytes. *Frontiers in Neuroscience*, 13:1125, 2019. Published 18 October 2019.

[97] Yukihiko Fujii, Shohei Maekawa, and Mitsuhiro Morita. Astrocyte calcium waves propagate proximally by gap junction and distally by extracellular diffusion of atp released from volume-regulated anion channels. *Scientific Reports*, 7:13115, 2017. Published 13 October 2017.

[98] Jack McNeill, Caleb Rudyk, Marion E. Hildebrand, and Natalina Salmaso. Ion channels and electrophysiological properties of astrocytes: Implications for emergent stimulation technologies. *Frontiers in Cellular Neuroscience*, 15:644126, 2021. Published 20 May 2021.

[99] Lionel F. Jaffe and Robbert Créton. On the conservation of calcium wave speeds. *Cell Calcium*, 24(1):1–8, 1998.

[100] 8w1e pet 8 well array. Accessed: September 2, 2024.

[101] P. R. F. Rocha, P. Schlett, L. Schneider, M. Dröge, V. Mailänder, H. L. Gomes, P. W. M. Blom, and D. M. de Leeuw. Low frequency electric current noise in glioma cell populations. *J. Mater. Chem. B*, 3:5035–5039, 2015.

[102] Pedro Rocha, Philipp Schlett, Uwe Kintzel, et al. Electrochemical noise and impedance of au electrode/electrolyte interfaces enabling extracellular detection of glioma cell populations. *Scientific Reports*, 6:34843, 2016. Published 06 October 2016.

[103] Tugba Palabas, Joaquín J. Torres, Matja Perc, and Muhammet Uzuntarla. Double stochastic resonance in neuronal dynamics due to astrocytes. *Chaos, Solitons & Fractals*, 168:113140, 2023.

[104] D. C. Lovelady, T. C. Richmond, A. N. Maggi, C.-M. Lo, and D. A. Rabson. Distinguishing cancerous from noncancerous cells through analysis of electrical noise. *Phys. Rev. E*, 76:041908, Oct 2007.

[105] A. Nightingale. Electrical noise from 'polarization cells' and from human tissues. *Nature*, 181:192–193, 1958. Published 18 January 1958.

[106] Ying Liu and Chunguang Li. Firing rate propagation through neuronalastrocytic network. *IEEE Transactions on Neural Networks and Learning Systems*, 24(5):789–799, 2013.

[107] Neil Joye, Alexandre Schmid, and Yusuf Leblebici. A cell-electrode interface noise model for high-density microelectrode arrays. In *2009 Annual International Conference of the IEEE Engineering in Medicine and Biology Society*, pages 3247–3250, 2009.

[108] Ralf Zeitler et al. Thermal noise as a probe for cell adhesion. *Biophysical Journal*, 96(3):298a, 2009.

[109] Moritz Voelker and Peter Fromherz. Nyquist noise of cell adhesion detected in a neuron-silicon transistor. *Phys. Rev. Lett.*, 96:228102, Jun 2006.

[110] R. Fabbri, A. Scidà, E. Saracino, et al. Graphene oxide electrodes enable electrical stimulation of distinct calcium signalling in brain astrocytes. *Nature Nanotechnology*, 2024. Published 10 July 2024.